

Calculation of optical- and acoustic-phonon-limited conductivity and Hall mobilities for *p*-type silicon and germanium

Frank Szmulowicz

University of Dayton Research Institute, 300 College Park Avenue, Dayton, Ohio 45469

(Received 25 May 1983)

Optical- and acoustic-phonon-limited mobilities for *p*-type silicon and germanium have been calculated, without the relaxation-time approximation, from solutions of the full Boltzmann equation. The valence-band dispersions are obtained from Kane's $6 \times 6 \vec{k} \cdot \vec{p}$ Hamiltonian. Hole-phonon transition rates are calculated using the deformation-potential theory with one adjustable parameter for hole-optical-phonon interaction strength which is fitted to mobility data at room temperature. This represents the first such calculation for silicon. Very good agreement is found between experiment and theory for both mobilities in silicon and for the conductivity mobility in germanium. The agreement between experiment and theory for the Hall factor in Ge is better than 20%, which may still be improved upon with more reliable deformation-potential parameters. However, the agreement is better than that attained by earlier calculations. The fitted values of the hole-optical-phonon deformation potentials are within bounds of independent estimates for their values. It may therefore be concluded that the deformation-potential theory is well suited for quantitative modeling of phonon-limited mobilities.

I. INTRODUCTION

Electrical transport measurements continue to be valuable tools for characterizing semiconductor materials and devices. In particular, Hall-effect measurements have become standard diagnostic tools in assessing material quality and in determining doping concentrations. The quantitative determination of concentrations from Hall data requires a knowledge of the so-called "r factor," the ratio of Hall to conductivity mobility. Rarely are Hall mobilities and conductivity mobilities obtained from the same sample. Ideally, these two parameters are obtained from the low and high magnetic field limits of the Hall mobility. Unfortunately, the high-field limit is often unattainable at elevated temperatures, due to the large magnetic fields required, for samples with low mobilities,¹ while the low-field limit is difficult to measure at low temperatures, for high-purity samples, owing to the lack of Hall-voltage signal resulting from too few thermal excited charge carriers.¹ It is often found that in these situations theoretical modeling can be of great utility.

A quantitative understanding of electrical transport properties is also of intrinsic interest since it can elucidate basic transport-limiting scattering mechanisms. Depending upon the material, its composition, and the temperature range studied, there can be several scattering mechanisms. In order to assess the influence of each mechanism it is convenient to deal with each one separately. In a previous paper the present author in collaboration with Madarasz investigated acoustic-phonon-limited mobilities in *p*-type silicon and germanium.^{2,3} With the use of deformation-potential concept,^{4,5} in conjunction with accurate band-shape models,⁶ mobilities were calculated from the full Boltzmann equation without the relaxation-time approximation.^{7,8} The degree of quantitative agreement attained by that calculation in comparison with experiments^{2,3} justifies the extension of transport modeling

to involve optical-phonon-limited transport with the same degree of rigor.

Phonon-limited transport in nonpolar *p*-type semiconductors, such as silicon and germanium, has been actively investigated for many years. Citations to papers dealing with the acoustic-phonon-limited transport in these materials are contained in Refs. 2 and 3. References 2 and 3 contained no adjustable parameters to characterize the strength of hole-acoustic-phonon interaction. In contrast, with the exception of the work by Tiersten^{4,5} and Lawaetz,⁹ the strength of the interaction is usually treated as an empirically adjustable parameter.

The optical-phonon scattering mechanisms and the resulting mobilities have been dealt with by many authors. Except for Lawaetz⁹ all these theoretical calculations have used the relaxation-time approximation and different degrees of band-shape approximations. The relaxation-time approximation results from retaining only the $l=1$ angular momentum component in a spherical harmonic expansion of the steady-state distribution function.¹⁰ In the present work $l=1, 3, 5,$ and 7 are used, thereby going beyond the relaxation-time approximation.

One of the earliest investigations of hole scattering by optical phonons was undertaken by Ehrenreich and Overhauser.¹¹ Matrix elements for scattering were considered for both the rigid- and deformable-ion models and spherical constant-energy surfaces. The matrix elements calculated by Ehrenreich and Overhauser were functions of the scattering angle only. This approach has since been superseded by the deformation-potential approach. The more exact model used in this paper considers the matrix elements as functions of both the incident- and scattered-hole directions within the deformation-potential model.

Another line of approach owes its origin to the deformation-potential concept introduced by Bardeen and Shockley.¹² Resulting expressions for nonpolar optical-phonon-limited mobilities were derived by Conwell.¹³

They are strictly valid for electrons in nondegenerate ellipsoidal bands. This approach is based on the relaxation-time approximation and phenomenological hole–optical-phonon coupling strengths.^{14,15} A good example of this approach is provided by the calculation of Lin, Li, Linares, and Teng¹⁶ for *p*-type silicon. These authors employ separate interband and intraband relaxation rates for the light- (*L*) and heavy- (*H*) hole bands based on a formalism developed by Bir, Normantas, and Pikus¹⁷ for the acoustic process, with optical-phonon–hole relaxation rates based on the work of Conwell.¹³ Lin *et al.* did not calculate a temperature-dependent *r* factor. A similar approach has been pursued by Hackmann, Neubert, Scherz, and Schlieff¹⁸ for *p*-type Si using *spherical* spin-orbit *S*-, *L*-, and *H*-hole bands, but with equal relaxation rates for the *L*- and *H*-hole bands, and no interband scattering with the *S*-hole band. Transition probabilities calculated by Hackmann *et al.* are taken from Wiley¹⁹ and are functions of scattering angle only. The resulting relaxation rates are similar to those of Herring and Vogt.²⁰ The *r* factor for *p*-type Si calculated by Hackmann *et al.*¹⁸ has an incorrect temperature dependence owing to the spherical-band approximation.

A simplifying approach due to Wiley¹⁹ reduces the complexity of the deformation-potential approach^{21,22} of Bir and Pikus. Here the transition probabilities are proportional to relevant deformation-potential constants (one for each phonon type) and an overlap matrix element between initial- and final-hole Bloch states. In Ref. 7 this approach has been criticized for neglecting the deformation-potential operator between these two states. The transition rates in Wiley's formulation¹⁹ are only functions of the scattering angle. This approach has been applied by Costato, Gagliani, Jacoboni, and Reggiani²³ to Si and Ge. The effect of the overlap correction was found to double the numerical value of the mobility as compared with calculations neglecting the overlap. The *r* factor was not calculated.

A good example of the phenomenological approach, in conjunction with the relaxation-time approximation, is given by the calculations performed by Nakagawa and Zukotynski.²⁴ Their relaxation rates involve two empirically adjustable deformation-potential constants—one for the acoustic and one for the optical process. In the work of Nakagawa and Zukotynski the scattering probabilities were assumed to be proportional to the density of the final states, and the effect of overlap between initial and final states was neglected. This makes the relaxation times equal for the *H*-hole and *L*-hole bands. The *r* factor of Nakagawa and Zukotynski for Ge is about 50% larger than measured and the *r* factor for Si does not match the experimental *r* factor at lower temperatures. The present calculation also regards the optical-phonon–hole interaction strength as adjustable (the acoustic-phonon–hole interaction is not adjustable, as explained in Refs. 2 and 3). The one adjustable parameter, d_0 , used here can in principle be related to experimental results from Raman scattering.²⁵ In this sense, the present theory could be pursued from “first principles” without any adjustment of parameters. An extension of the work of Nakagawa and Zukotynski, involving all three *S*-, *L*-, and *H*-hole bands of Si,

was performed by Takeda, Sakui, and Sakata.²⁶ The *r* factor calculated by Takeda *et al.*²⁶ for Si does not match the measured *r* factor due to their use of the simplified relaxation-time model.

A rather precise formulation of the hole–optical-phonon interaction has been put forward by Bir and Pikus²¹ on the basis of deformation-potential theory. They have derived expressions for the relevant matrix elements for a parabolic band model involving the top two valence bands of Si and Ge. Their results are analytic and by virtue of symmetry considerations require only one deformation-potential constant, d_0 , to characterize the strength of the interaction. The model of Bir and Pikus has subsequently been used by Lawaetz for *p*-type Ge.⁹ In Refs. 2 and 3 it was shown that the use of nonparabolic bands improves the calculated *r* factor in the acoustic-phonon–limited regime. The present paper will use a generalization of that theory by including all three top valence bands in calculating the scattering matrix elements.

In reviewing previous work on the subject of mobilities in *p*-type Si or *p*-type Ge it has become apparent that the degree of quantitative and even qualitative success has been limited.^{18,24,26} In a previous paper^{2,3} these limitations were found to be due to various band-shape approximations and the use of the relaxation-time approximation. In particular, there have been no reports of a successful calculation of the *r* factor for *p*-type Si over a wide temperature range, in spite of the use of empirically adjusted parameters. Typically, with two adjustable parameters for phonon-limited transport, if one adjusts the conductivity mobility to fit the data, the predicted Hall mobility often does not match experimental results.

The present work addresses the problem of phonon-limited mobilities employing an improved treatment of the crucial steps involved in the calculation. In Sec. II the theory of optical-phonon–hole scattering is reviewed and generalized to a nonparabolic band treatment. Section III contains a test of the calculational and theoretical procedures, and results for *p*-type Ge. Section IV is devoted to presentation of results for *p*-type Si. Finally, conclusions are presented.

II. DEFORMATION-POTENTIAL THEORY OF THE HOLE–OPTICAL-PHONON INTERACTION

The scattering rates for carriers interacting with optical phonons have been worked out within the deformation-potential picture by Bir and Pikus.^{21,27} The theory has been subsequently applied to Ge by Lawaetz.⁹ Bir and Pikus developed the formalism for the special case of two parabolic (*L*-hole and *H*-hole) valence bands, which results in relatively simple analytic expressions for the scattering rates. In what follows I shall summarize their theoretical development and extend it to the treatment of all six nonparabolic valence bands in diamond-type semiconductors.

A. Scattering operator

The potential experienced by a carrier in a lattice is composed of two parts. The first part corresponds to the

static equilibrium configuration of the lattice, $V_0(\vec{r})$ which is the part of the Hamiltonian employed in standard band-theory calculations, that is,

$$\left[-\frac{\hbar^2}{2m} \vec{\nabla}^2 + V_0(\vec{r}) \right] \psi_n(\vec{k}, \vec{r}) = E_n(\vec{k}) \psi_n(\vec{k}, \vec{r}) . \quad (2.1)$$

leading to the formation of bands $E_n(\vec{k})$ with associated Bloch wave functions $\psi_n(\vec{k}, \vec{r})$. In the presence of lattice vibrations atoms of the lattice are displaced from their equilibrium positions by the amount of $\vec{u}_{f\kappa}$. The index f labels the position of the unit cell, with mass M_0 , at \vec{R}_f and κ labels the location of the κ th basis atom, with mass M_κ , in the unit cell at $\vec{R}_{f\kappa}$. Bir and Pikus²⁷ assumed that the perturbation introduced by the presence of lattice vibrations depends on the instantaneous atom positions in the lattice and not their velocities; i.e., the adiabatic approximation. For small displacements from equilibrium the perturbation becomes

$$\delta V(\vec{r}) = \sum_{f,\kappa} \vec{\mathcal{V}}_{f\kappa}(\vec{r}) \cdot \vec{u}_{f\kappa} . \quad (2.2)$$

If only one atom at f,κ undergoes displacement \vec{u} we will have

$$\delta V(\vec{r}) = \vec{\mathcal{V}}_{f\kappa}(\vec{r}) \cdot \vec{u} \quad (2.3)$$

at point \vec{r} which is $\vec{r} - \vec{R}_f$ away from unit cell f . The lattice periodicity condition requires that an identical atom κ in the zeroth unit cell produces the same perturbation at a point $\vec{r} - \vec{R}_f$ away, which requires that

$$\vec{\mathcal{V}}_{0\kappa}(\vec{r} - \vec{R}_f) \cdot \vec{u} = \vec{\mathcal{V}}_{f\kappa}(\vec{r}) \cdot \vec{u} , \quad (2.4)$$

so that

$$\vec{\mathcal{V}}_{f\kappa}(\vec{r}) = \vec{\mathcal{V}}_{0\kappa}(\vec{r} - \vec{R}_f) \equiv \vec{\mathcal{V}}_{\kappa}(\vec{r} - \vec{R}_f) . \quad (2.5)$$

Altogether then,

$$\delta V(\vec{r}) = \sum_{f,\kappa} \vec{\mathcal{V}}_{\kappa}(\vec{r} - \vec{R}_f) \cdot \vec{u}_{f\kappa} . \quad (2.6)$$

Following Bir and Pikus²⁷ it is useful to define a cell's center-of-mass coordinate

$$\vec{u}_f = \sum_{\kappa} M_{\kappa} \vec{u}_{f\kappa} / \sum_{\kappa} M_{\kappa} , \quad (2.7)$$

and the relative displacements in cell f

$$\vec{u}_{f\kappa\kappa'} \equiv \vec{u}_{f\kappa} - \vec{u}_{f\kappa'} = -\vec{u}_{f\kappa'\kappa} . \quad (2.8)$$

In these coordinates Eq. (2.6) becomes

$$\delta V(\vec{r}) = \sum_f \vec{u}_f \cdot \vec{\mathcal{V}}(\vec{r} - \vec{R}_f) + \frac{1}{2} \sum_{f,\kappa,\kappa'} \vec{u}_{f\kappa\kappa'} \cdot \vec{\mathcal{V}}_{\kappa\kappa'}(\vec{r} - \vec{R}_f) , \quad (2.9)$$

where

$$\vec{\mathcal{V}}(\vec{r} - \vec{R}_f) = \sum_{\kappa} \vec{\mathcal{V}}_{\kappa}(\vec{r} - \vec{R}_f) \quad (2.10)$$

and

$$\vec{\mathcal{V}}_{\kappa\kappa'}(\vec{r} - \vec{R}_f) = \frac{1}{M_0} [\vec{\mathcal{V}}_{\kappa}(\vec{r} - \vec{R}_f) M_{\kappa'} - \vec{\mathcal{V}}_{\kappa'}(\vec{r} - \vec{R}_f) M_{\kappa}] . \quad (2.11)$$

Next we need to consider the range of the lattice-carrier interaction. Bir and Pikus²⁷ assumed that the perturbation at \vec{r} is determined principally by the motion of atoms nearest to the point \vec{r} , namely those atoms for which

$$|\vec{r} - \vec{R}_f| \ll \lambda , \quad (2.12)$$

where λ is the wavelength of lattice vibration. Furthermore, $\lambda \gg a_0$, where a_0 is the lattice constant, so that we are dealing with long-wavelength or short-wave-vector \vec{q} vibrations.

In the long-wavelength limit the center of mass of each cell for an optical mode does not move so that $\vec{u}_f = 0$ for all f in Eq. (2.9). Also in the same limit all sublattices move identically in each cell, which gives

$$\vec{u}_{f\kappa\kappa'} = \vec{u}_{\kappa\kappa'} = (\vec{u}_{\kappa} - \vec{u}_{\kappa'})_{\text{same cell}} , \quad (2.13)$$

so that

$$\delta V(\vec{r})_{\text{opt}} = \frac{1}{2} \sum_{\kappa\kappa'} \vec{u}_{\kappa\kappa'} \cdot \vec{\mathcal{V}}_{\kappa\kappa'}^{\text{opt}}(\vec{r}) , \quad (2.14)$$

where

$$\vec{\mathcal{V}}_{\kappa\kappa'}^{\text{opt}}(\vec{r}) \equiv \sum_f \vec{\mathcal{V}}_{\kappa\kappa'}(\vec{r} - \vec{R}_f) . \quad (2.15)$$

The c -number vector operator $\vec{\mathcal{V}}_{\kappa\kappa'}^{\text{opt}}(\vec{r})$ is a property of the lattice in equilibrium and has the periodicity of the lattice.

To proceed further, discrete atomic displacements $\vec{u}_{f\kappa}$ are taken over to the continuum limit. This is accomplished by observing that in the long-wavelength limit the discrete displacement of the atom $f\kappa$ at a distance $|\vec{r} - \vec{R}_{f\kappa}| \ll \lambda$ from the field point \vec{r} differs only slightly from the average displacement $\vec{u}_{\kappa}(\vec{r})$ of the κ th sublattice at \vec{r} . One may then expand each $\vec{u}_{f\kappa}$ in a series with respect to $\vec{r} - \vec{R}_{f\kappa}$. For acoustic vibrations the first two terms in the series are retained. For optical vibrations only the first term is kept, that is,

$$\vec{u}_{f\kappa} = \vec{u}_{\kappa}(\vec{r}) . \quad (2.16)$$

Equation (2.14) can be specialized to the case of the diamond lattice, where for identical atoms in the unit cell

$$M_1 = M_2 = M , \quad (2.17a)$$

$$M_0 = M_1 + M_2 = 2M , \quad (2.17b)$$

so that from Eqs. (2.8), (2.11), and (2.14)

$$\delta V(\vec{r})_{\text{opt}} = \frac{1}{2} [\vec{u}_1(\vec{r}) - \vec{u}_2(\vec{r})] \cdot \vec{\mathcal{V}}^{\text{opt}}(\vec{r}) , \quad (2.18)$$

where

$$\begin{aligned} \vec{\mathcal{V}}^{\text{opt}}(\vec{r}) &\equiv \sum_f \vec{\mathcal{V}}_{12}(\vec{r} - \vec{R}_f) \\ &= \sum_f [\vec{\mathcal{V}}_1(\vec{r} - \vec{R}_f) - \vec{\mathcal{V}}_2(\vec{r} - \vec{R}_f)] . \end{aligned} \quad (2.19)$$

A symmetry analysis of the operators in Eq. (2.18) leads to great simplifications in the subsequent treatment. The optical mode in the diamond-structure semiconductors is threefold degenerate and transforms according to rows of the Γ_{25}^+ irreducible representation of the diamond space group $O_h^7 (Fd3m)$. The relative displacements

$$\vec{u}_1(\vec{r}) - \vec{u}_2(\vec{r}) \equiv \vec{z}(\vec{r}) \quad (2.20)$$

behave then as axial vectors, or pseudovectors, being even on inversion. Since $\mathcal{Y}^{\text{opt}}(\vec{r})$ is the property of the lattice in thermal equilibrium, it is independent of \vec{z} , and is translationally invariant. If the two atoms in a cell are interchanged via the inversion operation, the potential $\delta V(\vec{r})_{\text{opt}}$ cannot change. Since \vec{z} is an axial vector, the invariance of $\delta V(\vec{r})_{\text{opt}}$ implies that \mathcal{Y}^{opt} is an axial vector as well.²⁷ For selection-symmetry purposes the angular behavior of the operator $\mathcal{Y}^{\text{opt}}(\vec{r})$ is that of the basis functions for the Γ_{25}^+ representation of O_h^7 . This completes the derivation and exploration of properties of the scattering operator for the hole-optical-phonon interaction

$$\delta V(\vec{r})_{\text{opt}} = \frac{1}{2} \vec{z}(\vec{r}) \cdot \mathcal{Y}^{\text{opt}}(\vec{r}). \quad (2.21)$$

B. Transition rates

The transition-matrix element for optical-phonon-hole scattering between Bloch states of bands n and m with wave vectors \vec{k} and \vec{k}' , respectively, with phonon-occupation numbers N in the initial and N' in the final states, is given by

$$\langle n, \vec{k}; N | \frac{1}{2} \vec{z}(\vec{r}) \cdot \mathcal{Y}^{\text{opt}}(\vec{r}) | m, \vec{k}'; N' \rangle. \quad (2.22)$$

Here

$$\langle \vec{r} | n, \vec{k} \rangle = \psi_n(\vec{k}, \vec{r}) = e^{i\vec{k} \cdot \vec{r}} u_n(\vec{k}, \vec{r})$$

is the Bloch wave with the cell periodic part $u_n(\vec{k}, \vec{r})$. The relative displacement field $\vec{z}(\vec{r}) = \vec{u}_1 - \vec{u}_2$ in a quantized form becomes

$$\vec{z} = \vec{z}_1 - \vec{z}_2 = \sum_{\vec{q}, s} [\bar{p}_1(\vec{q}, s) - \bar{p}_2(\vec{q}, s)] a_s(\vec{q}) e^{i\vec{q} \cdot \vec{r}} + \text{c.c.}, \quad (2.23)$$

where \vec{q} is the phonon wave vector, s is the polarization branch, $a_s(\vec{q})$ is the phonon destruction operator, and c.c. denotes complex conjugation. In the long-wavelength limit the polarization vectors $\bar{p}_\kappa(\vec{q}, s)$ are given by²⁷

$$\bar{p}_1(\vec{q}, s) = -\bar{p}_2(\vec{q}, s) \equiv \bar{p}(\vec{q}, s), \quad (2.24)$$

since the two atoms vibrate 180° out of phase. Trivially, we can choose for the three polarization branches

$$\bar{p}(\vec{q}, s) = \hat{e}_s, \quad (2.25)$$

i.e., unit vectors in the s th direction.

The transition-matrix element for the s th polarization branch now becomes

$$\begin{aligned} & \langle n, \vec{k}; N | T_s | m, \vec{k}'; N' \rangle \\ &= \sum_{\vec{q}} \langle n, \vec{k}; N | [a_s(\vec{q}) e^{i\vec{q} \cdot \vec{r}} + a_s^\dagger(\vec{q}) e^{-i\vec{q} \cdot \vec{r}}] \\ & \quad \times (\hat{e}_s \cdot \mathcal{Y}^{\text{opt}}) | m, \vec{k}'; N' \rangle. \end{aligned} \quad (2.26)$$

Inserting a complete set of states between the phonon operators and \mathcal{Y}^{opt} results in

$$\begin{aligned} & \sum_{\vec{q}, n', \vec{k}''} \left[\frac{\hbar n_{\vec{q}s}}{2\rho\omega_{\vec{q}s}\Omega} \right]^{1/2} \langle n, \vec{k} | e^{i\vec{q} \cdot \vec{r}} | n', \vec{k}'' \rangle \\ & \quad \times \langle n', \vec{k}'' | \hat{e}_s \cdot \mathcal{Y}^{\text{opt}} | m, \vec{k}' \rangle \delta_{N, N'-1} \end{aligned} \quad (2.27)$$

for scattering with absorption of an optical phonon, and

$$\begin{aligned} & \sum_{\vec{q}, n', \vec{k}''} \left[\frac{\hbar(n_{\vec{q}s} + 1)}{2\rho\omega_{\vec{q}s}\Omega} \right]^{1/2} \langle n, \vec{k} | e^{-i\vec{q} \cdot \vec{r}} | n', \vec{k}'' \rangle \\ & \quad \times \langle n', \vec{k}'' | \hat{e}_s \cdot \mathcal{Y}^{\text{opt}} | m, \vec{k}' \rangle \delta_{N, N'+1} \end{aligned} \quad (2.28)$$

for the case of phonon emission. The factors in the square root contain the phonon-occupation number

$$n_{\vec{q}s} = \left[\exp \left(\frac{\hbar\omega_{\vec{q}s}}{k_B T} \right) - 1 \right]^{-1}, \quad (2.29)$$

where $\omega_{\vec{q}s}$ is the phonon frequency, k_B is the Boltzmann constant, T is the absolute temperature, ρ is the mass density of the crystal, and Ω is its volume.

In Eqs. (2.27) and (2.28) $\mathcal{Y}^{\text{opt}}(\vec{r})$ has the periodicity of the lattice so that

$$\langle n', \vec{k}'' | \hat{e}_s \cdot \mathcal{Y}^{\text{opt}} | m, \vec{k}' \rangle = \langle n', \vec{k}'' | \mathcal{Y}_s^{\text{opt}} | m, \vec{k}' \rangle \delta_{\vec{k}, \vec{k}''},$$

where $(\vec{r} | n, \vec{k}) = u_n(\vec{k}, \vec{r})$ is the cell periodic part of $\langle \vec{r} | n, \vec{k} \rangle$. On the other hand,

$$\langle n, \vec{k} | e^{\pm i\vec{q} \cdot \vec{r}} | n', \vec{k}' \rangle = \delta_{\vec{k}, \vec{k}' \pm \vec{q}}(n, \vec{k} | n', \vec{k}').$$

For small wave vectors the optical branch for diamond-type semiconductors is dispersionless,

$$\omega_{\vec{q}s} = \omega_0,$$

for all three polarization branches. Therefore,

$$\begin{aligned} & \langle n, \vec{k}; N | T_s^\pm | m, \vec{k}'; N' \rangle \\ &= \sum_{n'} \left[\frac{\hbar(n_0 + \frac{1}{2} \mp \frac{1}{2})}{2\rho\omega_0\Omega} \right]^{1/2} \langle n, \vec{k} | n', \vec{k}' \rangle \\ & \quad \times \langle n', \vec{k}' | \mathcal{Y}_s^{\text{opt}}(\vec{r}) | m, \vec{k}' \rangle \delta_{N, N' \mp 1}, \end{aligned} \quad (2.30)$$

where T_s^+ , T_s^- represent absorption and emission, respectively. The last formal step is to note that the cell periodic parts $| n, \vec{k} \rangle$ satisfy the closure relation

$$\sum_n | n, \vec{k} \rangle \langle n, \vec{k} | = 1 \quad (2.31)$$

for a fixed wave vector. With this important simplification we finally arrive at

$$\begin{aligned} \langle n, \vec{k}; N | T_s^\pm | m, \vec{k}'; N' \rangle \\ = \left[\frac{\hbar(n_0 + \frac{1}{2} \mp \frac{1}{2})}{2\rho\omega_0\Omega} \right]^{1/2} (n, \vec{k} | \mathcal{Y}_s^{\text{opt}}(\vec{r}) | m, \vec{k}') \delta_{N, N' \mp 1}. \end{aligned} \quad (2.32)$$

I would like to observe that Refs. 4 and 7 do not make use of relation (2.31) in calculating the acoustic-phonon-hole scattering rates. Instead, the sum over intermediate states n' is carried over the top six valence bands. In the paper by Madarasz and Szmulowicz, $1 \leq n' \leq 6$, but clearly Eq. (2.15) of Ref. 7 is better written, using Eq. (2.31), as

$$B_{nm}^j(\vec{k}, \vec{k}') = 2(n, \vec{k} | D^j | m, \vec{k}'). \quad (2.33)$$

A numerical test of the alternative procedure, Eq. (2.33), for germanium has shown that the two methods agree to at least four significant figures. The six-band set, as was surmised,⁷ is complete enough for the acoustic-phonon transition rates among the top valence bands. It is more satisfying, and more accurate in all cases, to use Eq. (2.33) instead of Eq. (3.9) of Ref. 4 or Eq. (2.15) of Ref. 7.

Returning back to the discussion of transition rates, the transition probability per unit time from Fermi's golden rule is given by

$$\begin{aligned} P^\pm(n, \vec{k}; m, \vec{k}') = \frac{2\pi}{\hbar} \left[\frac{\hbar(n_0 + \frac{1}{2} \mp \frac{1}{2})}{2\rho\omega_0\Omega} \right] \\ \times \sum_s | (n, \vec{k} | \mathcal{Y}_s^{\text{opt}} | m, \vec{k}') |^2 \\ \times \delta(E_n(\vec{k}) - E_m(\vec{k}') \pm \hbar\omega_0), \end{aligned} \quad (2.34)$$

where the contributions from all three polarization branches have been summed. In Eq. (2.34) n and m will range from 1 to 6 for the three doubly degenerate top valence bands. The transition probability appropriate for scattering among the doubly degenerate manifolds is obtained by summing over its members, so that

$$P^\pm(N, \vec{k}; M, \vec{k}') = \frac{2\pi(n_0 + \frac{1}{2} \mp \frac{1}{2})}{2\rho\omega_0\Omega a_0^2} \left[\frac{3}{2} d_0^2 \sum_s \sum_{n(N)m(M)} \left| \sum_{p,q} a_{np}^*(\vec{k}) | \epsilon_{pqs} | a_{mq}(\vec{k}') \right|^2 \right] \delta(E_N(\vec{k}) - E_M(\vec{k}') \pm \hbar\omega_0). \quad (2.38)$$

The factor in the parentheses is identically $U^0(M\vec{k}, N\vec{k}')$ in the four-band model in Eq. (2.30) of Ref. 9. The analytic result for the four-band model is given in Eq. (B1) of Appendix B.

Owing to the inelastic nature of the hole-optical-

$$\begin{aligned} P^\pm(N, \vec{k}; M, \vec{k}') \\ = \frac{1}{2} \frac{2\pi}{\hbar} \left[\frac{\hbar(n_0 + \frac{1}{2} \mp \frac{1}{2})}{2\rho\omega_0\Omega} \right] \\ \times \sum_s \sum_{n(N)m(M)} | (n, \vec{k} | \mathcal{Y}_s^{\text{opt}} | m, \vec{k}') |^2 \\ \times \delta(E_N(\vec{k}) - E_M(\vec{k}') \pm \hbar\omega_0), \end{aligned} \quad (2.35)$$

where $N=1,2,3$ stands for the S -, L -, and H -hole bands with corresponding Kramer's degenerate doublets: $N(1)=N(2)=1$, $N(3)=N(4)=2$, and $N(5)=N(6)=3$; conversely, $n(1)=1,2$, $n(2)=3,4$, and $n(3)=5,6$. The factor of $\frac{1}{2}$ in front of Eq. (2.35) has been said to represent the sum over the final states and an average over the initial states for the manifolds N and M .^{4,11,21} This I feel might be misleading since it implies that this averaging is the property of the transition rates. I show in Appendix A that the factor of $\frac{1}{2}$ is due to the structure of the Boltzmann equation and not of the transition rates.

Explicit evaluation of Eq. (2.35) requires the input of the periodic parts of the Bloch wave functions $(\vec{r} | n, \vec{k})$. In the present calculation these are obtained from the solution of the 6×6 Kane's $\vec{k} \cdot \vec{p}$ Hamiltonian.⁶ The solutions take the form

$$| n, \vec{k} \rangle = \sum_{p=1}^6 a_{np}(\vec{k}) | \epsilon_p \rangle, \quad (2.36)$$

where $(\vec{r} | \epsilon_p)$ transform as $x \uparrow, y \uparrow, z \uparrow, x \downarrow, y \downarrow$, and $z \downarrow$ for $p=1-6$, respectively. Thus $(\vec{r} | \epsilon_p)$ transforms according to the Γ_{25}^{opt} representation of O_h , with both spins included. Since $\mathcal{Y}_x^{\text{opt}} \sim x$, $\mathcal{Y}_y^{\text{opt}} \sim y$, and $\mathcal{Y}_z^{\text{opt}} \sim z$ behave as polar vectors in each atomic subcell, there is only one nonzero matrix element possible on the basis of symmetry. If r, t , and s stand for Cartesian coordinates, then the nonzero matrix elements are^{21,27}

$$(\epsilon_r | \mathcal{Y}_t^{\text{opt}} | \epsilon_s) \equiv (d_0/a_0)\sqrt{3} | \epsilon_{rts} |, \quad (2.37)$$

as long as r and s refer to the same spin. d_0 is the only parameter characterizing the strength of the hole-optical-phonon interaction used in the present work, a_0 is the lattice constant, ϵ_{rts} represents the Levi-Civita density and d_0 will be treated as an adjustable parameter in a way to be described later.

To make contact with the earlier four-band model of Bir and Pikus,²¹ I rewrite Eq. (2.35), using Eqs. (2.36) and (2.37), in the following form:

phonon scattering,

$$P^\pm(N, \vec{k}; M, \vec{k}') \neq P^\pm(M, \vec{k}'; N, \vec{k}). \quad (2.39)$$

On the other hand, it is clear from Eq. (2.38) that

$$U^0(M, \vec{k}; N, \vec{k}') = U^0(N, \vec{k}'; M, \vec{k}) . \quad (2.40)$$

If one examines the structure of the 6×6 Kane's $\vec{k} \cdot \vec{p}$ Hamiltonian with spin-orbit splitting,⁶ one observes that the matrix elements are quadratic in \vec{k} since inversion is a symmetry operation for diamond-type semiconductors. The time-reversal symmetry gives

$$E_n(\vec{k}) = E_n(-\vec{k}) . \quad (2.41)$$

In addition, from the structure of the $\vec{k} \cdot \vec{p}$ Hamiltonian the solutions $a_{np}(\vec{k})$ in Eq. (2.36) have the property that

$$a_{np}(\vec{k}) = a_{np}(-\vec{k}) . \quad (2.42)$$

Therefore, Eq. (2.38) has the additional symmetry

$$\begin{aligned} P^\pm(N, \vec{k}; M, \vec{k}') &= P^\pm(N, \vec{k}; M, -\vec{k}') \\ &= P^\pm(N, -\vec{k}; M, \vec{k}') , \end{aligned} \quad (2.43)$$

which is called the momentum randomization. This property will be important in setting up solutions to the Boltzmann equation, which will be discussed next.

C. Solution of the Boltzmann equation

The general form of the Boltzmann equation is [see Eq. (A10)]

$$\begin{aligned} &\left[\frac{e}{\hbar} \vec{F} \cdot \vec{\nabla}_{\vec{k}} - \frac{e}{\hbar^2} \vec{B} \cdot [\vec{\nabla}_{\vec{k}} E_N(\vec{k}) \times \vec{\nabla}_{\vec{k}}] \right] f_N(\vec{k}) \\ &= \sum_M \frac{\Omega}{(2\pi)^3} \int d\vec{k}' \left[P(M, \vec{k}'; N, \vec{k}) f_M(\vec{k}') \left[1 - \frac{f_N(\vec{k})}{2} \right] - P(N, \vec{k}; M, \vec{k}') f_N(\vec{k}) \left[1 - \frac{f_M(\vec{k}')}{2} \right] \right] , \end{aligned} \quad (2.44)$$

where \vec{F} and \vec{B} are the electric and magnetic fields, respectively, and P is the sum of transition rates from all scattering processes. For the acoustic-phonon process, assumed to be elastic, the microscopic reversibility holds

$$P_{ac}(M, \vec{k}'; N, \vec{k}) = P_{ac}(N, \vec{k}; M, \vec{k}') , \quad (2.45)$$

so that the $f_M(\vec{k}') f_N(\vec{k})$ cross terms in Eq. (2.44) vanish. Clearly, for the acoustic process only the scattering term assumes the form

$$\sum_M \frac{\Omega}{(2\pi)^3} \int d\vec{k}' P_{ac}(N, \vec{k}; M, \vec{k}') [f_M(\vec{k}') - f_N(\vec{k})] . \quad (2.46)$$

In thermal equilibrium the Fermi-Dirac distribution is a function of energy only. Since $E_M(\vec{k}') = E_N(\vec{k})$ in the acoustic process, the scattering term, Eq. (2.46), vanishes in thermal equilibrium.

For the optical-phonon process, using the energy-conservation condition, one can obtain the following structure for the scattering terms:

$$\begin{aligned} &U^0(E_N, E_N + \hbar\omega) f(E_N + \hbar\omega) \left[1 - \frac{f(E_N)}{2} \right] (n+1) + U^0(E_N, E_N - \hbar\omega) f(E_N - \hbar\omega) \left[1 - \frac{f(E_N)}{2} \right] n \\ &- U^0(E_N, E_N - \hbar\omega) f(E_N) \left[1 - \frac{f(E_N - \hbar\omega)}{2} \right] (n+1) - U^0(E_N, E_N + \hbar\omega) f(E_N) \left[1 - \frac{f(E_N + \hbar\omega)}{2} \right] n , \end{aligned} \quad (2.47)$$

where U^0 's are given by the large parentheses in Eq. (2.38). It is easy to show that for the optical process the scattering term vanishes only if f is the thermal equilibrium Fermi-Dirac distribution and n is the Bose-Einstein equilibrium phonon distribution.²⁸

In the nondegenerate case one may assume $f^2 \ll f$ which eliminates cross terms in the collision term, Eq. (2.44), and allows one to facilitate further analytical developments. With the elimination of cross terms in Eq. (2.44) the scattering term for the optical process vanishes if n is the Bose-Einstein distribution but f now is the Boltzmann distribution.²⁸ The scattering term for the optical process, in the nondegenerate case, now becomes

$$\sum_M \frac{\Omega}{(2\pi)^3} \int d\vec{k}' [P_{opt}(M, \vec{k}'; N, \vec{k}) f_M(\vec{k}') - P_{opt}(N, \vec{k}; M, \vec{k}') f_N(\vec{k})] . \quad (2.48)$$

Since we will be interested only in the odd-parity "current-carrying" parts of f we can simplify Eq. (2.48) further. $f_M(\vec{k}')$ is odd in \vec{k}' , and $P_{opt}(M, \vec{k}'; N, \vec{k})$, by virtue of the momentum randomization, is even in \vec{k}' . Therefore, the first term in Eq. (2.48), also called the "in-scattering" term, vanishes identically in the *present* model of optical-phonon—hole scattering.^{9,29} This is a very crucial simplification since all the hole-distribution functions can now be evaluated at a single energy $E_N(\vec{k})$. The in-scattering term would have required one to evaluate $f_M(\vec{k}')$ at $E_N(\vec{k}) \pm \hbar\omega_0$ and no simple procedure exists for dealing with this case.²⁸

All angle-dependent quantities are expanded in cubic-harmonics series:

$$P_{NM}^{\text{ac}}(\vec{k}, \vec{k}') = \frac{\pi k_B T}{2\Omega\hbar} \left[\sum_i \sum_{L,L'} A_{NL,ML'}^i(E_N(\vec{k})) \left[\sum_{\mu=1}^{l_i} K_L^{i\mu}(\hat{k}) K_{L'}^{i\mu}(\hat{k}') \right] \delta(E_N(\vec{k}) - E_M(\vec{k}')) \right], \quad (2.49)$$

$$P_{NM}^{\text{opt}}(\vec{k}, \vec{k}')^{\pm} = \frac{\pi d_0^2}{\rho\omega_0\Omega a_0^2} (n_0 + \frac{1}{2} \mp \frac{1}{2}) \sum_{L,L'} B_{LL'}^{\alpha}(E_N(\vec{k}), E_M(\vec{k}')) K_L^{\alpha}(\hat{k}) K_{L'}^{\alpha}(\hat{k}') \delta(E_N(\vec{k}) - E_M(\vec{k}') \mp \hbar\omega_0). \quad (2.50)$$

The steady-state distribution function is expanded in fields F and B as

$$f_N(\vec{k}) = f_N^0(\vec{k}) [1 + \vec{F} \cdot \vec{\Phi}_N(\vec{k}) + (\vec{F} \times \vec{B}) \cdot \vec{X}_N(\vec{k})], \quad (2.51)$$

with

$$\vec{\Phi}_N(\mathcal{E}, \hat{k}) = \sum_{\lambda} e \left[\frac{4\pi}{k_B T} \right]^2 \vec{K}_{\lambda}^{\delta}(\hat{k}) \theta_{N\lambda}^{\delta}(\mathcal{E}, T) \quad (2.52)$$

and

$$\vec{X}_N(\mathcal{E}, \hat{k}) = \sum_{\lambda} \left[\left[\frac{4\pi}{k_B T} \right]^3 \frac{4\pi e^2}{\hbar} \right] \vec{K}_{\lambda}^{\delta}(\hat{k}) \xi_{N\lambda}^{\delta}(\mathcal{E}, T). \quad (2.53)$$

Here $K_L^{i\mu}(\hat{k})$ is the cubic harmonic for the μ th row of the i th irreducible representation of O_h , with angular momentum index L , in direction \hat{k} . The expansion coefficients A for the acoustic process are functions of a single energy. For the optical process the expansion coefficients B are functions of both the initial- and final-hole energies. Owing to the momentum randomization only even representations occur in P^{opt} . Of these only the invariant Γ_1 or α representation coefficients are needed.²⁹ The field expansion, Eq. (2.51), for $f_N(\vec{k})$ was derived in an earlier publication.^{2,3} The "vector" cubic harmonic $\vec{K}_{\lambda}^{\delta}$ is defined as

$$\vec{K}_{\lambda}^{\delta}(\hat{k}) = \begin{pmatrix} K_{\lambda}^{\delta x}(\hat{k}) \hat{e}_x \\ K_{\lambda}^{\delta y}(\hat{k}) \hat{e}_y \\ K_{\lambda}^{\delta z}(\hat{k}) \hat{e}_z \end{pmatrix}, \quad (2.54)$$

since the rows of the $\Gamma_{15} = \delta$ representation can be labeled with Cartesian coordinates.

A solution of the Boltzmann equation will yield the energy-dependent expansion coefficients θ and ξ in Eqs. (2.52) and (2.53). Equation (2.46) in conjunction with Eq. (2.48) constitutes the collision term of the Boltzmann equation. Multiplying both sides of the Boltzmann equation by

$$K_{\lambda}^{\delta y}(\hat{k}) \delta(\mathcal{E} - E_N(\vec{k})) d\vec{k} \quad (2.55)$$

and integrating over \vec{k} yields a system of linear equations for θ and ξ . These are

$$G_{N\lambda'}^{\delta}(\mathcal{E}) = \sum_{M,\lambda''} S_{N\lambda'',M\lambda'}^{\delta}(\mathcal{E}, T) \theta_{M\lambda''}^{\delta}(\mathcal{E}, T), \quad (2.56)$$

$$[S_{N\lambda'',M\lambda'}^{\delta}(\mathcal{E})]_{\text{ac}} = \sum_{L,L'} \left\{ \langle j, \nu, \lambda'' | \Gamma_N(\mathcal{E}) | j, \nu, L \rangle A_{NL,ML'}^j \langle j, \nu, L' | \Gamma_M(\mathcal{E}) | j, \nu, \lambda' \rangle - \delta_{NM} \sum_{P=1}^3 \langle j, \nu, \lambda''; j, \nu, \lambda' | \Gamma_N(\mathcal{E}) | \alpha, L \rangle A_{NL,PL}^{\alpha} \langle \alpha, L' | \Gamma_P(\mathcal{E}) | 1 \rangle \right\}, \quad (2.64)$$

$$\begin{aligned} & \frac{1}{3} \sum_{\lambda''} \theta_{N\lambda''}^{\delta}(\mathcal{E}, T) \mathcal{H}_{N\lambda'',N\lambda'}^{\delta}(\mathcal{E}) \\ & = \sum_{M,\lambda''} S_{N\lambda'',M\lambda'}^{\delta}(\mathcal{E}, T) \xi_{M\lambda'}^{\delta}(\mathcal{E}, T). \end{aligned} \quad (2.57)$$

The field-term matrices were derived in Ref. 3 to be

$$G_{N\lambda''}^{\delta}(\mathcal{E}) = -\frac{2}{l_{\delta}} \sum_{\mu=1}^{l_{\delta}} \int d\hat{k} K_{\lambda''}^{\delta\mu}(\hat{k}) \Gamma_N(\mathcal{E}, \hat{k}) \times \left[\frac{\partial E_N(\vec{k})}{\partial k_{\mu}} \right]_{E_N(\vec{k}) = \mathcal{E}} \quad (2.58)$$

and

$$\mathcal{H}_{N\lambda'',N\lambda'}^{\delta}(\mathcal{E}) = \sum_{\nu', \nu'', \mu'} \epsilon_{\nu' \nu'' \mu'} \times \langle \delta, \nu', \lambda'' | \Gamma_N(\mathcal{E}) h_p^N(\mathcal{E}) | \delta, \mu', \lambda' \rangle, \quad (2.59)$$

where $l_{\delta} = 3$ (dimensionality of the Γ_{15} representation). Also

$$\Gamma_N(\mathcal{E}, \hat{k}) = \left[\frac{2m_0}{\hbar^2} \right]^{3/2} \gamma_N^{1/2}(\mathcal{E}, \hat{k}) \frac{d\gamma_N(\mathcal{E}, \hat{k})}{d\mathcal{E}}, \quad (2.60)$$

with

$$\frac{\hbar^2 k_N^2}{2m_0} = \gamma_N(E_N(\vec{k}), \hat{k}) \quad (2.61)$$

being the solution of the cubic equation³ for band calipers k_N of band N in direction \hat{k} , ϵ is the Levi-Civita density, and

$$h_p^N(\mathcal{E}, \hat{k}) = \hat{e}_p \cdot [\vec{\nabla}_{\vec{k}} E_N(\vec{k}) \times \vec{\nabla}_{\vec{k}}]_{E_N(\vec{k}) = \mathcal{E}} \quad (2.62)$$

is the operator evaluated on the constant $E_N(\vec{k}) = \mathcal{E}$ energy surface. The bra-kets denote solid-angle integrals in the Brillouin zone.

The "scattering" matrix S is a sum of scattering matrices for the acoustic and optical processes. A derivation analogous to that of Ref. 3 leads to the following definition:

$$S_{N\lambda'',M\lambda'}^{\delta}(\mathcal{E}, T) = [S_{N\lambda'',M\lambda'}^{\delta}(\mathcal{E})]_{\text{ac}} + [S_{N\lambda'',M\lambda'}^{\delta}(\mathcal{E}, T)]_{\text{opt}}. \quad (2.63)$$

Here, as in Ref. 3, for the acoustic process

which from the matrix-element theorem³⁰ is in fact independent of the partner index ν . The optical scattering term is diagonal in band indices and is given by

$$[S_{N\lambda'',M\lambda'}^{j\nu}(\mathcal{E},T)]_{\text{opt}} = -D\delta_{NM} \sum_{L,L',P=1}^3 \langle j,\nu,\lambda'',j,\nu,\lambda' | \Gamma_N(\mathcal{E}) | \alpha,L \rangle \\ \times [(n_0+1)B_{NL,PL'}^\alpha(\mathcal{E},\mathcal{E}-\hbar\omega_0) \langle \alpha L' | \Gamma_P(E-\hbar\omega_0) | 1 \rangle \\ + n_0 B_{NL,PL'}^\alpha(\mathcal{E},\mathcal{E}+\hbar\omega_0) \langle \alpha L' | \Gamma_P(\mathcal{E}+\hbar\omega_0) | 1 \rangle]. \quad (2.65)$$

D is a material-dependent constant

$$D = \frac{2d_0^2\hbar^2}{k_B T \rho(\hbar\omega_0)a_0^2} \equiv \frac{\bar{d}_0^2}{t} \mathcal{D} \quad (2.66)$$

(measured in Ry a.u.³), where \bar{d}_0 is the numerical value of d_0 in Ry and t is the numerical value of T in K. For germanium with parameters in Table I

$$\mathcal{D}_{\text{Ge}} = 2.345 \times 10^3$$

(measured in Ry a.u.³), and for silicon with parameters in Table I

$$\mathcal{D}_{\text{Si}} = 3.400 \times 10^3$$

(measured in Ry a.u.³), where a.u. is the Bohr radius. Selection rules used in deriving Eq. (2.65) project out only the $\Gamma_1=\alpha$ components of $B^{j\nu}$.

Note that the matrix $S_{N\lambda'',M\lambda'}(\mathcal{E},T)$, Eq. (2.63), is symmetric in the combined $(N\lambda'',M\lambda')$ indices, a useful property for matrix manipulations. The first term in S_{opt} is for optical-phonon emission, $\mathcal{E} \rightarrow \mathcal{E} - \hbar\omega_0$, and the second for phonon absorption, $\mathcal{E} \rightarrow \mathcal{E} + \hbar\omega_0$. The temperature dependence of θ in Eq. (2.56) and ξ in Eq. (2.57) is entirely due to D and n_0 in S_{opt} . Additional integrals, not appearing in the acoustic case, in Eq. (2.65)

$\langle \alpha L' | \Gamma_P(\mathcal{E} \pm \hbar\omega_0) | 1 \rangle$ are evaluated by methods outlined in Ref. 3.

D. Transport coefficients

The conductivity and Hall mobilities are evaluated using Eqs. (2.53a) and (2.53b) of Ref. 3. In the more streamlined notation of the present paper we have

$$\mu_c = -\frac{e}{2\hbar} \left[\frac{4\pi}{k_B T} \right]^2 \frac{\sum_{N\lambda} \int d\mathcal{E} e^{-\beta\mathcal{E}} \theta_{N\lambda}^\delta(\mathcal{E},T) G_{N\lambda}^\delta(\mathcal{E})}{4\pi \sum_N \int_0^\infty d\mathcal{E} e^{-\beta\mathcal{E}} \langle \alpha_0 | \Gamma_N(\mathcal{E}) | \alpha_0 \rangle}, \quad (2.67)$$

$$r\mu_c^2 = -\frac{2\pi e^2}{\hbar} \left[\frac{4\pi}{k_B T} \right]^3 \frac{\sum_{N\lambda} \int d\mathcal{E} e^{-\beta\mathcal{E}} \xi_{N\lambda}^\delta(\mathcal{E},T) G_{N\lambda}^\delta(\mathcal{E})}{\sum_N \int_0^\infty d\mathcal{E} e^{-\beta\mathcal{E}} \langle \alpha_0 | \Gamma_N(\mathcal{E}) | \alpha_0 \rangle}. \quad (2.68)$$

Results for Ge and Si using the formalism developed above are presented in Secs. III and IV. The temperature range covered is from 10 to 400 K. There are valid questions concerning the use of the equipartition approxima-

TABLE I. Experimental input parameters.

Quantity	Notation	Si	Ge
Band parameters (dimensionless)	A	-4.27 ^a	-13.27 ^b
	B	-0.63 ^a	-8.63 ^b
	C	4.93 ^a	12.4 ^b
Deformation potentials (eV)	a	2.1 ^c	2.0 ^b
	b	-2.2 ^c	-2.1 ^b
	d	-5.3 ^c	-7.0 ^b
	ρ	2.328 ^d	5.3267 ^d
Phonon parameters (dyn/cm ²)	ρc^2	18.852 $\times 10^{11}$ ^c	1.53 $\times 10^{12}$ ^b
	$c = \text{phonon speed}$	ρc^2	6.804 $\times 10^{11}$ ^c
Spin-orbit splitting (meV)	Δ	44.0 ^e	300 ^b
Lattice constant (Å)	a_0	5.430 86 ^d	5.657 48 ^d
Optical-phonon energy (meV)	$\hbar\omega_0$	63 ^d	37 ^d

^aReference 24.

^bReference 5.

^cReference 19.

^dReference 31.

^eReference 32.

tion at lower temperatures in the acoustic-phonon treatment. In Appendix C it is shown that in reality another approximation is used which is accurate to better than 1%.

III. RESULTS FOR GERMANIUM

Acoustic- and optical-phonon-limited mobility for germanium has been calculated previously by Lawaetz⁹ in the four-band parabolic band approximation.²¹ Results presented in this section were obtained using all of the top six valence bands with the material parameters used by Lawaetz.⁹ Therefore, this section not only presents a comparison between the two calculations but also serves as

a check on the accuracy of the parabolic band model. Several of its shortcomings were pointed out in Refs. 2 and 3 for the acoustic-limited mobility.

A. Hole—optical-phonon transition probabilities

The hole—optical-phonon transition probabilities were calculated using the formalism developed in Sec. II. For comparison with the analytic results of Bir and Pikus²¹ in the case of parabolic bands it is useful to list the quantity $U^0(N, \hat{k}; M, \hat{k}')$. The expression for $U^0(N, \hat{k}; M, \hat{k}')$ in the parabolic model is given by Eq. (B1) in Appendix B. The corresponding general result in the six-band model is given in Eq. (2.38). Table II presents the comparison for

TABLE II. Comparison between numerical results for $U^0(N, \hat{k}; M, \hat{k}')$ in the four-band model, Eq. (B1), and the six-band model, Eq. (2.38). $U^0(N, \hat{k}; M, \hat{k}')$ is in units of d_0^2 . The incident hole's energy is $\mathcal{E} = 0.0135/17$ eV and the scattered hole's energy is $\mathcal{E} + \hbar\omega_0$.

Scattering directions	Bands	Six-band model present work	Four-band model of Bir and Pikus (Ref. 21)
[100]→[100]	$H \rightarrow H$	0.0000	0
	$L \rightarrow L$	0.0168	0
	$H \rightarrow L$	3.0000	3
	$L \rightarrow H$	3.0000	3
[100]→[010]	$H \rightarrow H$	2.2500	9/4
	$L \rightarrow L$	2.2548	9/4
	$H \rightarrow L$	0.7632	3/4
	$L \rightarrow H$	0.7500	3/4
[100]→[111]	$H \rightarrow H$	1.5000	3/2
	$L \rightarrow L$	1.5126	3/2
	$H \rightarrow L$	1.5126	3/2
	$L \rightarrow H$	1.5000	3/2
[111]→[111]	$H \rightarrow H$	0.9999	1
	$L \rightarrow L$	0.7551	1
	$H \rightarrow L$	2.2653	2
	$L \rightarrow H$	2.0049	2
[110]→[110]	$H \rightarrow H$	1.1304	0.8352
	$L \rightarrow L$	0.6696	0.8352
	$H \rightarrow L$	2.3460	2.1648
	$L \rightarrow H$	1.9212	2.1648
[100]→[321]	$H \rightarrow H$	0.9978	0.9344
	$L \rightarrow L$	0.9564	0.9344
	$H \rightarrow L$	2.0664	2.0655
	$L \rightarrow H$	2.0178	2.0655
[111]→[111]	$H \rightarrow H$	1.6668	5/3
	$L \rightarrow L$	1.7649	5/3
	$H \rightarrow L$	1.2615	4/3
	$L \rightarrow H$	1.3317	4/3
[110]→[110]	$H \rightarrow H$	1.6161	1.6701
	$L \rightarrow L$	1.8849	1.6701
	$H \rightarrow L$	1.1421	1.3299
	$L \rightarrow H$	1.4208	1.3299
[100]→[110]	$H \rightarrow H$	1.3389	1.1955
	$L \rightarrow L$	1.2228	1.1955
	$H \rightarrow L$	1.7994	1.8045
	$L \rightarrow H$	1.7055	1.8045
[110]→[111]	$H \rightarrow H$	1.2378	1.2360
	$L \rightarrow L$	1.1130	1.2360
	$H \rightarrow L$	1.9083	1.7637
	$L \rightarrow H$	1.7661	1.7637

several selected scattering directions between the H - and L -hole bands.

The four-band model entries in Table II which are rational numbers are exact results independent of band parameters B , C , and D . Other entries do depend on these parameters which along with other parameters used in this calculation for germanium are given in Table I. The results in Table II indicate that the intraband and interband scattering probabilities are of comparable magnitude and are significantly anisotropic. In general, results involving the H -hole band are more in agreement with the analytic four-band model than the results involving the less parabolic L -hole band.

The transition probabilities for the acoustic and optical scattering processes were calculated on the same scattering directions and energy meshes as in Refs. 2, 3, and 8. That is, 128 (\hat{k}, \hat{k}') progenitor directions were used for one direction mesh and a larger 250 (\hat{k}, \hat{k}') progenitor-directions mesh was used for the other. Two separate energy meshes were used. The small energy mesh had a spacing of 0.0135/17 eV with 16 energies with this mesh size. The second mesh had a spacing of 0.0045 eV and 52 energies with this mesh size, up to the maximum hole energy of 0.234 eV. Since the split-off energy in germanium is 0.3 eV, and $\hbar\omega_0 = 0.037$ eV, transitions involving the S -hole band were not calculated. The maximum energy of 0.234 eV is estimated to provide sufficient accuracy to calculate μ_c and μ_H up to 400 K, somewhat above the temperature where high-purity germanium becomes intrinsic.

The acoustic- and optical-phonon-hole scattering rates were fitted to a double-cubic-harmonic series as described in Ref. 8. Twenty-four cubic-harmonic pairs were used to represent angular variations of the rates, at each calculated energy, in both the incident and scattered hole directions. The cubic harmonics in the fit were, in the Von der Lage and Bethe³³ notation, $\alpha_0, \alpha_4, \alpha_6, \alpha_8, \delta_1, \delta_3, \delta_5, \delta_7, \delta_7'$, and the maximum combined angular momentum of the cubic harmonics was $L + L' = 8$. Note that other cubic harmonics were not used in the fit since they are not needed in the calculation of the scattering matrix, Eq. (2.63). Also, note the addition of two new cubic harmonics, δ_7 and δ_7' , in order to improve convergence of various angular momentum sums, Eqs. (2.49)–(2.53), (2.56), (2.57), (2.64), (2.65), (2.67), and (2.68). Since δ_7 and δ_7' were not calculated in Ref. 33, I provide below their functional dependence in the notation of Ref. 33:

$$\delta_7 = \frac{3 \times 11 \times 13}{16} \sqrt{15} \left\{ z^7 - \frac{21}{13} [\delta_{5z}] - \frac{35}{33} [\delta_{3z}] - \frac{1}{3} [\delta_{1z}] \right\}, \quad (3.1)$$

$$\delta_7' = \frac{13}{2} \sqrt{5 \times 7 \times 11} \left\{ z(x^6 + y^6) + \frac{5}{8} [\delta_{7z}] - \frac{15}{13} [\delta_{5z}'] - \frac{45}{52} [\delta_{5z}] + \frac{5}{11} [\delta_{3z}] - \frac{2}{11} [\delta_{1z}] \right\}. \quad (3.2)$$

Several checks performed with the above forms for δ_7 and δ_7' indicated that they agree with their spherical harmonic forms derived by Altmann and Cracknell.³⁴

In Appendix B it is shown that the cubic-harmonic decomposition of $U^0(N, \hat{k}; M, \hat{k}')$ for the Γ_1 representation

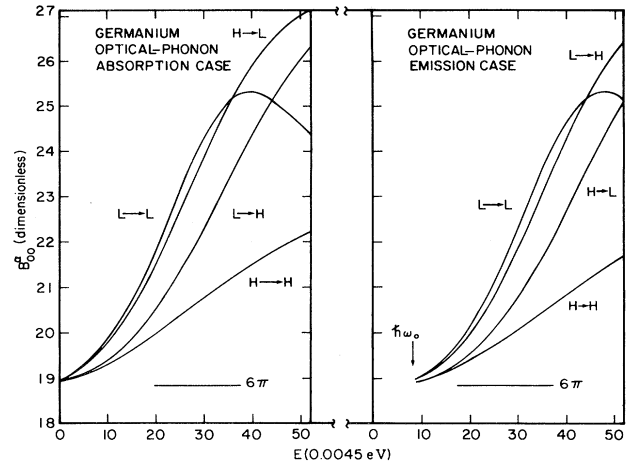


FIG. 1. Energy dependence of the isotropic expansion coefficients, Eq. (2.50), for the optical-phonon-hole transition rates in Ge: optical-phonon absorption, left panel; optical-phonon emission, right panel. The optical-phonon energy $\hbar\omega_0 = 0.037$ eV. H and L represent the heavy- and light-hole bands, respectively.

has only one nonzero coefficient,

$$B_{LL'}^\alpha = 6\pi \delta_{L0} \delta_{L'0}, \quad (3.3)$$

for both emission and absorption, which is independent of energy. The cubic-harmonic fitting in the double series of the present rates yields the fitting coefficients shown in Fig. 1 as a function of the incident hole's energy. It is only at the lowest energies that the expansion coefficient B_{00}^α approaches the parabolic-band result of 6π . Otherwise, B_{00}^α is a strong, yet smooth, function of the incident hole's energy. From Eq. (2.40)

$$U^0(M, \vec{k}, E_M(\vec{k}); N, \vec{k}', E_N(\vec{k}')) = U^0(N, \vec{k}', E_N(\vec{k}'); M, \vec{k}, E_M(\vec{k})), \quad (3.4)$$

so that the expansion coefficients must also satisfy the relation

$$B_{ML, NL'}^\alpha(\mathcal{E}, \mathcal{E} + \hbar\omega_0) = B_{NL', ML}^\alpha(\mathcal{E} + \hbar\omega_0, \mathcal{E}). \quad (3.5)$$

$B_{ML, NL'}^\alpha(\mathcal{E}, \mathcal{E} + \hbar\omega_0)$ refers to the hole in band M at energy \mathcal{E} absorbing one optical phonon in going to band N at energy $\mathcal{E} + \hbar\omega_0$. $B_{NL', ML}^\alpha(\mathcal{E} + \hbar\omega_0, \mathcal{E})$ refers to the hole in band N at energy $\mathcal{E} + \hbar\omega_0$ emitting one optical phonon in going to band M at energy \mathcal{E} . In Fig. 1 $L = L' = 0$ so that the absorption and emission curves are identical except for the permutation of the band indices and the shift of the emission curves by $\hbar\omega_0$ with respect to the absorption curves.

As the consequence of the coefficients B being larger than 6π , Fig. 1, the optical-phonon scattering is stronger than predicted by the four-band model of Bir and Pikus²¹ for the same value of the optical deformation potential d_0 . Nevertheless, mobilities calculated with the two models should agree since the difference between the B 's in Fig. 1 and 6π , for the more important emission case, is not greater than 5% at lower energies. The expansion coefficients for other Γ_1 cubic-harmonic pairs such as α_0, α_4 ,

$\alpha_4\alpha_4$, $\alpha_0\alpha_6$, and $\alpha_0\alpha_8$ are less than 0.1 for all energies examined; other even representations were not employed in the fit. Therefore, as far as the mobility calculations are concerned, the optical-phonon scattering produces isotropic scattering rates in germanium.

B. Mobility results for germanium

The formalism developed in Sec. II was employed for calculation of μ_c and μ_H in *p*-type Ge. Unlike the case when the acoustic-phonon scattering acts alone, when both the acoustic and optical processes are present together, one cannot factor out all of the temperature-dependent factors in Eqs. (2.52) and (2.53). In Ref. 3 it was possible to calculate energy-dependent quantities only once. Here one must calculate all the quantities at all energies and as a function of temperature.

For purposes of interpolating integrands in the numerators of equations for the two mobilities, Eqs. (2.67) and (2.68), it is useful to know an analytic form for the low-energy behavior of the integrands. Using the same arguments as those leading to Eqs. (3.4)–(3.8) of Ref. 3, one can show that the integrand in the numerator of Eq. (2.67), for parabolic bands and in the present model at low energies, behaves as

$$\frac{\mathcal{E}^2}{\bar{a}\mathcal{E} + \bar{b}(n_0/T)[(\mathcal{E} + \hbar\omega_0)\mathcal{E}]^{1/2}}, \quad (3.6)$$

where \bar{a} and \bar{b} are parameters to be obtained from a numerical fit to the integrand. Similarly, the integrand in the numerator of Eq. (2.68) behaves at low energies as

$$\frac{\mathcal{E}^2\sqrt{\mathcal{E}}}{\{\bar{c}\mathcal{E} + (\bar{d}n_0/T)[\mathcal{E}(\mathcal{E} + \hbar\omega_0)]^{1/2}\}^2}, \quad (3.7)$$

with two other fitting parameters \bar{c} and \bar{d} . The two terms in the denominator reflect the contributions of the acoustic- and optical-absorption processes, respectively. At higher energies, $\mathcal{E} > \hbar\omega_0$, the optical-emission processes become operative so that in the parabolic-band model an additional term,

$$\frac{n_0+1}{T}[\mathcal{E}(\mathcal{E} - \hbar\omega_0)]^{1/2}\Theta(\mathcal{E} - \hbar\omega_0), \quad (3.8)$$

where Θ is the Heaviside step function, will appear in the denominators of Eqs. (3.6) and (3.7). Therefore, the integrands suffer a discontinuity in slope which requires caution in interpolating the integrands. The slope discontinuity is of course present in the more exact six-band model employed here. At higher temperatures though, the discontinuity becomes small due to the $1/T$ dependence in Eq. (3.8). This is also the region where the optical-phonon emission becomes important in the transport coefficients calculation, Eqs. (2.67) and (2.68). When necessary the interpolation was performed via the Lagrange method.³⁵ All integrations involving the Boltzmann factor were done using the 25-point Gauss-Laguerre integration.³⁶

The present and Lawaetz's implementations of the optical deformation theory for the calculation of galvanomagnetic coefficients employ one adjustable parameter—the optical deformation potential constant d_0 . There are in-

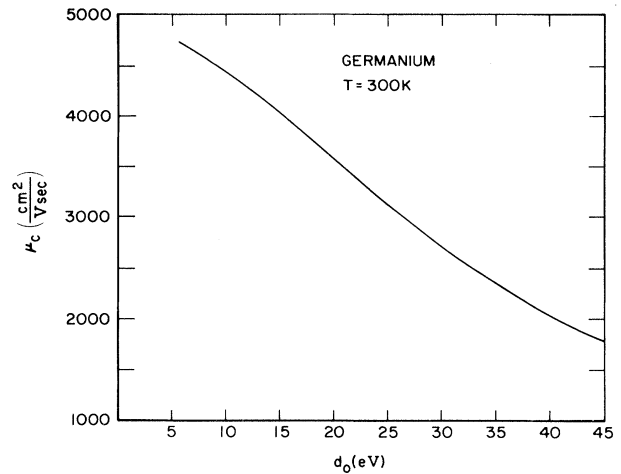


FIG. 2. Conductivity mobility in germanium as a function of the optical-phonon–hole interaction strength parameter d_0 at 300 K, with parameters of Table I.

dependent estimates of the magnitude of d_0 which place its value for most group IV and III-V semiconductors in the (30–40)-eV range.²⁵ Figure 2 shows the calculated value of μ_c as a function of d_0 for germanium at 300 K. As d_0 increases the optical-phonon scattering becomes stronger so that the mobility decreases. If one were to use the approximation

$$\frac{1}{\mu} = \frac{1}{\mu_{ac}} + \frac{1}{\mu_{opt}}, \quad (3.9)$$

given that $\mu_{opt} \sim d_0^{-2}$, then one would expect that $\mu \sim d_0^{-2}$ in the region where the optical-phonon scattering is the dominant mobility limiting mechanism. In fact, Fig. 2 exhibits this behavior for $d_0 > 25$ eV.

To proceed further one must choose a particular value for d_0 based on a measured value of μ_c or μ_H at some high temperature. The 300 K temperature is convenient to use given the large strength of optical-phonon interaction and optical-phonon population at this temperature. Unfortunately, there are a number of $\mu_c(300\text{ K})$ values quoted in the published literature. One of the earliest values is given by Prince³⁷ as $\mu_c(300\text{ K}) = 1820\text{ cm}^2/\text{V sec}$ from drift-mobility measurements, a minority carrier experiment. Brown and Bray¹⁵ give $\mu_c(300\text{ K}) = 2060\text{ cm}^2/\text{V sec}$ from conductivity measurements. This number depends crucially on the assumption that the hole concentration in their samples is constant from 77 K on up and that the strong field limit has been attained below 77 K with 7-kG fields. The $\mu_c(300\text{ K})$ value is extrapolated from $T < 260\text{ K}$ data since their sample 112A went intrinsic above this temperature.¹⁵ The time-of-flight measurements of Ottaviani, Canali, Nava, and Mayer³⁸ on high-purity Ge can be extrapolated from $T < 220\text{ K}$ data to yield $\mu_c(300\text{ K}) = 2245\text{ cm}^2/\text{V sec}$. This again is a minority carrier experiment.

Lawaetz⁹ uses the Brown and Bray¹⁵ value of μ_c to fit d_0 for which he obtains $d_0 = (6.41 \pm 0.03)\text{ eV}$. In another publication, though, Lawaetz³⁹ states that Ref. 9 obtains $d_0 \simeq 40\text{ eV}$. I surmise that the former value is the square

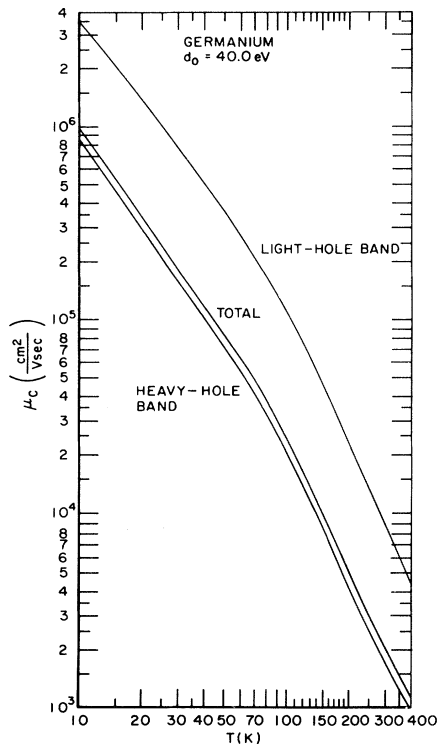


FIG. 3. Calculated total and partial conductivity mobilities in germanium using $d_0=40.0$ eV and parameters of Table I as a function of temperature.

root of the latter. Reggiani *et al.*⁴⁰ cite Lawaetz as having said that $d_0=40.25$ eV. Thus indirectly it appears that d_0 in Ref. 9 is about 40 eV. This is consistent with tabulations for d_0 of Wiley.¹⁹ From Fig. 1, $d_0=44.1$ eV will yield $\mu_c(300\text{ K})=1820$ cm²/V sec of Prince,³⁷ $d_0=36.5$ eV will yield $\mu_c(300\text{ K})=2244$ cm²/V sec of Ottaviani *et al.*,³⁸ and $d_0=40.0$ eV will yield $\mu_c(300\text{ K})=2060$ cm²/V sec of Brown and Bray.¹⁵ This last value is very close to that obtained by Lawaetz.⁹ This agreement is due to the fact that the coefficients displayed in Fig. 1 do not differ by more than 5% from the 6π value used by Lawaetz for transitions involving the H -hole band below 0.09 eV. The H band will be shown to dominate μ_c and the Boltzmann integral for μ_c , Eq. (2.68), is well con-

TABLE III. Ratios of band contributions to the conductivity tensors in germanium, $d_0=40.0$ eV, as a function of temperature. σ_{11}^N and σ_{123}^N are defined in Eq. (3.11). p_H and p_L are thermal band occupancies.

T (K)	$\sigma_{11}^H/\sigma_{11}^L$	$\sigma_{123}^L/\sigma_{123}^H$	p_H/p_L
10	6.06	1.06	24.79
50	4.69	1.60	23.72
100	4.39	1.86	23.32
150	4.21	2.04	23.00
200	4.13	2.15	22.66
250	4.11	2.22	22.22
300	4.14	2.26	21.64
350	4.19	2.29	20.88
400	4.25	2.31	20.27

verged by 0.09 eV.

In Ref. 9 Lawaetz approximately corrects for nonparabolicity of the bands but not for the concomitant effect on the transition rates. If the correction is dropped, d_0 fitted by Lawaetz⁹ rises to 6.53 eV. Therefore, the band-shape nonparabolicity alone appears to lower the value of d_0 .

Figure 3 shows the total and partial conductivity mobilities for germanium, where the partial band mobilities are defined as

$$\mu_{c,H} = \frac{\sum_{N=1}^3 \mu_{c,HPN}^N}{\sum_N p_N}, \quad (3.10)$$

for the choice of $d_0=40.0$ eV, which gives $\mu_c=2060$ cm²/V sec of Brown and Bray¹⁵ at 300 K. From effective mass considerations, $m_L/m_H \approx \frac{1}{8}$, one expects $\mu_{c,H}^L$ to be greater than $\mu_{c,H}^H$. The overall contributions of the bands to the conductivity tensors²⁴

$$\sigma_{11} = ep\mu_c$$

and

$$\sigma_{123} = ep\mu_c\mu_H$$

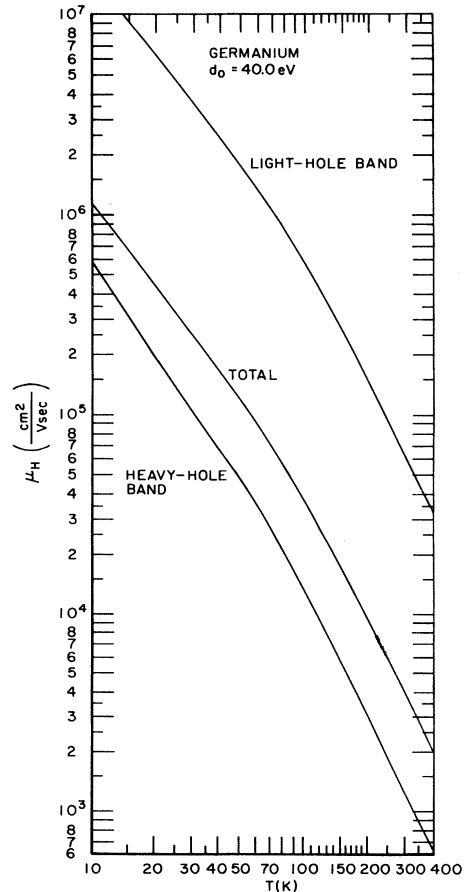


FIG. 4. Calculated total and partial Hall mobilities in germanium for $d_0=40.0$ eV and parameters of Table I as a function of temperature.

are given by

$$\sigma_{11}^N = e\mu_c^N p_N \quad (3.11a)$$

and

$$\sigma_{123}^N = (e\mu_c)\mu_H^N p_N, \quad (3.11b)$$

that is, σ_{11}^N and σ_{123}^N are proportional to numerators of Eq. (3.10). By including the band occupancy factors, p_N , the conductivity tensors give a better picture of each band's contribution to the current. In Table III the ratios of conductivity tensors for the light-hole and heavy-hole bands are displayed at selected temperatures. The overall contribution of the heavy-hole band to the σ_{11} tensor is only four times that of the light-hole band even though the heavy-hole band has about 20 times as many holes as the light-hole band. Nakagawa and Zukotynski²⁴ give $\sigma_{11}^H/\sigma_{11}^L = 3.45$ at 60 K and 3.70 at 300 K.

Figure 4 presents the decomposition of the Hall mobility into its partial-band mobilities. The light-hole band becomes the dominant band by about a factor of 2 as can be seen from the second column of Table III. At 60 K Nakagawa and Zukotynski provide $\sigma_{123}^L/\sigma_{123}^H = 2.69$ at 60 K and 2.73 at 300 K.

Figure 5 gives the comparison between the measured and calculated conductivity mobilities. It is intended that only the data of Brown and Bray¹⁵ ($N_A = 1.25 \times 10^{13}$ cm⁻³) be used for critical comparison since $d_0 = 40.0$ eV fits their 300 K μ_c mobility. The agreement between experiment and theory is seen to be very good. At 30 K there is an indication that the data exhibit the effect of ionized impurity scattering. The break in slope at the onset of strong optical-phonon emission around 70 K is well

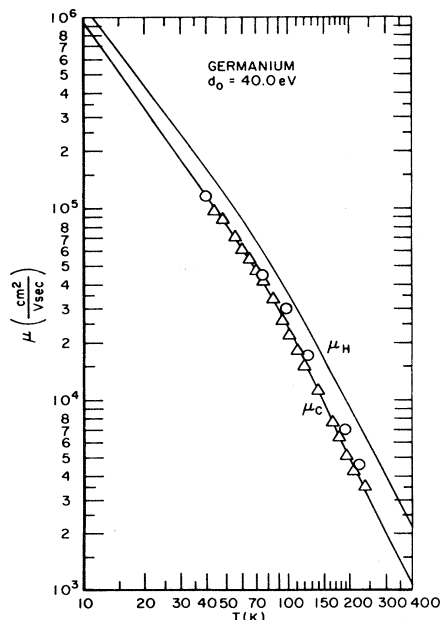


FIG. 5. Calculated and experimental conductivity and Hall mobilities for *p*-type Ge in the phonon-limited regime. The circles represent time-of-flight data of Ottaviani *et al.* (Ref. 38) $|N_A - N_D| \approx 2 \times 10^{10}$ cm⁻³ and triangles represent data of Brown and Bray (Ref. 15) $N_A - N_D = 1.25 \times 10^{13}$ cm⁻³.

predicted by theory, as well as are the shape and magnitude of the curve for $T > 70$ K. Beyond 200 K the calculated curve decreases in slope. This is a common feature of several mobility calculations for Ge.^{15,40} Caution needs to be exercised in interpreting this feature as being real. One is dealing here with high-energy holes for which the $6 \times 6 \vec{k} \cdot \vec{p}$ extrapolation may not hold with the same accuracy as at lower-hole energies. For example, at 0.2 eV the heavy-hole wave vector is one-eighth of the Γ -X Brillouin-zone distance. The degree of agreement with μ_H data will be discussed with reference to Fig. 6 for the *r* factor.

The *r* factor for germanium is shown in Fig. 6 together with the data of Goldberg *et al.*⁴¹ and Beer and Willardson.⁴² The general effect of adding the optical-phonon scattering is to raise the *r* factor from the value it had for the acoustic-phonon scattering process, $d_0 = 0$ eV. The calculated $r(81 \text{ K}) = 1.45$ may be compared with the calculated acoustic-phonon value³ of 1.43 and the value of 1.36 ± 0.07 of Beer and Willardson.⁴² The influence on these results due to the uncertainties in the deformation potentials *a*, *b*, and *d* have already been discussed in Ref. 3. A gratifying feature in the results of Fig. 6 is that the addition of the optical-phonon processes has resulted in the correct shape for the *r* vs *T* curve as compared with the data of Goldberg *et al.*⁴¹ The discrepancy in the overall magnitudes is due to several factors. First, the deformation potential for Ge, especially $d = -7$ eV, is not as well known as in Si. The value of the deformation-potential parameter *a* is also in doubt.⁹ This affects μ_H more than it does μ_c since μ_H is calculated by using the scattering matrix twice. Second, with $N_A - N_D = 2 \times 10^{13}$ cm⁻³ the sample *D* of Goldberg *et al.* must be affected by ionized impurity scattering which lowers the *r* value.²⁴ Third, at higher temperatures Ge, with its small band gap, is affected by the presence of electrons which again lowers the "apparent" hole *r* factor. This is well illustrated in Fig. 3 of Goldberg *et al.*⁴¹ by contrasting the behavior of sample *D* ($N_A - N_D = 2 \times 10^{13}$ cm⁻³) and sample *G* ($N_A - N_D = 3.4 \times 10^{14}$). The *r* factor for sample *D* is higher than that for sample *G* when $T < 200$ K because it is less affected by the ionized impurity scattering. For

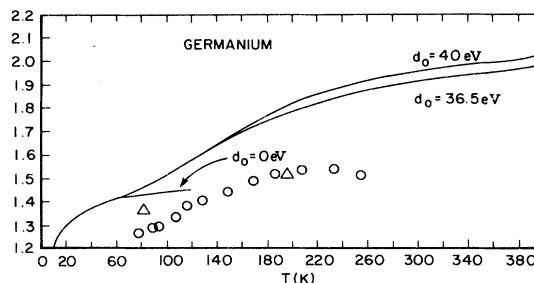


FIG. 6. Calculated and experimental *r* factor for *p*-type Ge in the phonon-limited regime. The $d_0 = 0$ eV curve gives the result for the acoustic-phonon scattering. The triangles represent sample *C* of Beer and Willardson (Ref. 42) $N_A - N_D = 1 \times 10^{13}$ cm⁻³ and the circles represent Goldberg, Adams, and Davis (Ref. 41) sample *D*, $N_A - N_D = 2.4 \times 10^{13}$ cm⁻³. The data point of Beer and Willardson (Ref. 42) at 196 K is from a sample with $N_A - N_D = 2 \times 10^{14}$ cm⁻³.

$T > 200$ K the situation is reversed because of the larger p/n ratio in sample *G*. The falloff of the r factor for sample *D* in Fig. 6 is due to the intrinsic electrons.

Nevertheless, the difference in magnitude between experiment and theory in Fig. 6 is less than 20% for $T < 200$ K. The r factor of Nakagawa and Zukotynski²⁴ for Ge varies between 1.95 at 50 K and 2.2 at 200 K. The r factor of Lawaetz⁹ has generally the same shape as the calculated r factor in Fig. 6 but is greater in magnitude since Lawaetz's $r(81 \text{ K}) \approx 1.6 - 1.7$. It has been the experience of the previous calculation³ that the r factor decreases as the band nonparabolicity is included in the band dispersions and in calculating the scattering rates. By neglecting the latter, Lawaetz's r factor is larger than the r factor shown in Fig. 6. This point will be discussed further in Sec. IV with comparison to the calculation and data for p -type Si.

Figure 7 shows the calculated temperature exponents $\alpha_{c,H}$ for both mobilities

$$\mu_{c,H}(T) \sim T^{-\alpha_{c,H}(T)}. \quad (3.12)$$

At low temperatures $\alpha_c \sim 1.5$ consistent with the parabolic band value (μ_c is dominated by the more parabolic heavy-hole band). This is observed in the data of Brown and Bray¹⁵ and Ottaviani *et al.*³⁸ The least parabolic band L produces the deviation from 1.5 in α_H at low temperatures. At higher temperatures experiments show that $\alpha_c = 2.3$ (Goldberg *et al.*,⁴¹ Brown and Bray,¹⁵ Ottaviani *et al.*³⁸), while Morin⁴³ gives $\alpha_c = 2.33$. From the calculated α_c it appears that 2.3 is an average α_c for $100 < T < 300$ K. For $T > 200$ K α_c decreases due to the decrease in slope discussed in connection with Fig. 5 for μ_c . Goldberg *et al.*⁴¹ also provide $\alpha_H \sim 2.1$ in the optical-phonon-limited region which is closely reflected in Fig. 7. The temperature exponents are then found to be predicted satisfactorily in both the acoustic- and optical-phonon-dominated temperature regions.

Overall, this section has shown that the present calculation agrees in the optical region with the earlier calculation⁹ for μ_c while improving on earlier calculations^{9,24} for μ_H and r . The 20% discrepancy in the r factor is due to inadequacies of parameters used to represent the

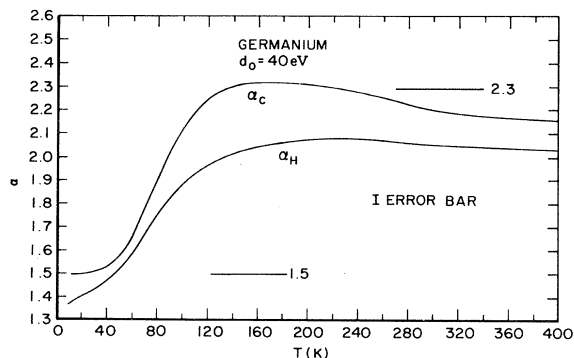


FIG. 7. Calculated temperature exponents (dimensionless) of the phonon-limited mobilities in p -type Ge. The error bar gives the estimated accuracy of extracting exponents when $T > 250$ K from 5-K interval data.

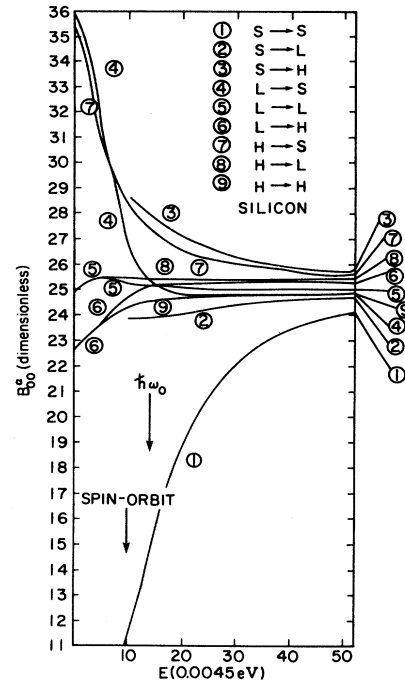


FIG. 8. Energy dependence of the isotropic expansion coefficients, Eq. (2.50), for the optical-phonon-hole transition rates in silicon. The optical-phonon energy is $\hbar\omega_0 = 0.063$ eV. H , L , and S stand for the heavy, light, and spin-orbit hole bands. The case of scattering with phonon absorption is depicted.

acoustic-phonon region since the optical-phonon contributions to the r factor adds onto the r factor for the acoustic process in Fig. 6.

IV. RESULTS FOR SILICON

A. Hole-optical-phonon transition possibilities

The quantities $B_{N0,M0}^\alpha(\mathcal{E}, \mathcal{E} + \hbar\omega_0)$ for phonon absorption, Eq. (2.50), in silicon are shown in Fig. 8. First, one observes that these quantities are not equal to 6π in any energy limit. Second, most of the energy variations occur for energies less than the spin-orbit energy. Beyond the spin-orbit energy the expansion coefficients $B_{N0,M0}^\alpha$ are effectively constant except for those NM band pairs which involve the spin-orbit band S . The symmetry principle Eq. (3.5), exemplified in Fig. 1 for Ge, can be used to obtain the corresponding curves for the case of phonon emission. Silicon parameters used to calculate $B_{NL,ML}^\alpha$ are given in Table I. An examination of calculated $B_{NL,ML}^\alpha$ indicates that although the coefficients for $L = L' = 0$ are always the largest, on the order of 20, nonspherical contributions can be on the order of unity. Typically, this occurs for transitions involving the S -hole band, otherwise the nonspherical contributions are on the order of 10^{-2} . By and large, then the optical-phonon scattering can also be regarded as being isotropic in p -type Si.

The lack of similarity between Figs. 1 and 8 for Ge and Si, respectively, has its roots in different valence-band dispersions for these materials. For Ge-hole energies of

interest, $\mathcal{E} < 0.25$ eV, are still less than the spin-orbit splitting energy, while for Si they are 6 times that energy. As a result, silicon bands attain their parabolic $E \sim k^2$ behavior for smaller values of k^2 , and therefore at smaller energies than in germanium.^{6,44} In the parabolic band limit the coefficients $B_{NL,ML}^{\alpha}$ are known to be energy independent^{9,21} since the wave functions are only directionally dependent. Given the large optical-phonon energy, $\hbar\omega_0 = 0.063$ eV, for Si, at least one of the bands in Fig. 8 must be above the spin-orbit energy, which is not the case with Ge where $\hbar\omega_0 = 0.037$ eV. It is therefore desirable to exercise some caution in accepting uncritically the band dispersions of Kane at the substantial energies used in the present and other calculations.⁴⁴

B. Mobility results for silicon

The formalism already outlined and presented in Sec. III for p -type Ge has been applied to p -type Si. Rather than fitting various energy dependences for low energies in numerators and denominators of Eqs. (2.67) and (2.68), as was done for Ge, Eqs. (3.6)–(3.8), all energy-dependent quantities for Si were calculated on a logarithmic energy mesh as well as on a linear-energy mesh. The linear mesh size was 0.045 eV with 52 energies and the log mesh was given by

$$\mathcal{E} = \exp[-13.305 + (j-1)0.6]$$

(measured in eV), with $1 < j < 16$. The interpolating forms were checked out and were found to be quite valid for Si as well. Same directions in \hat{k} space were used to calculate the rates for Si as for Ge, and the same least-squares fitting procedure for the transition rates was implemented.

With one fitting parameter d_0 the mobilities and the r factor displayed in Fig. 9 were obtained. The d_0^{-2} dependence of μ_c and μ_H is approximately followed for larger d_0 . The 300-K r factor varies between 0.78 and 0.70 for

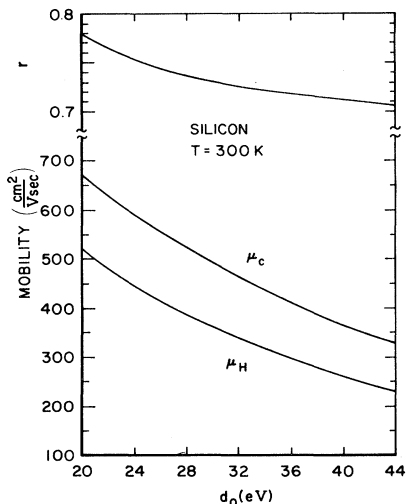


FIG. 9. Conductivity mobility, Hall mobility, and the r factor in p -type Si in the phonon-limited regime as a function of the hole-optical-phonon deformation potential d_0 at 300 K. Material parameters from Table I are used.

TABLE IV. Published values of 300 K mobilities in high-purity p -type Si and of temperature exponents of the mobilities.

μ_c (cm ² /V sec)	α_c	μ_H (cm ² /V sec)	α_H
495 ^a	2.3 ^{a,b}	425 ^c	
480 ± 15 ^d	2.7 ± 0.1 ^d	369 ^e	2.93 ^e
504 ^f		398 ^g	2.91 ^g
478 ^h	2.24 ^h	370 ⁱ	2.91 ⁱ
		412 ^j	

^aReference 45.

^bReference 49.

^cReference 50.

^dReference 46.

^eReference 1.

^fReference 47.

^gReference 51.

^hReference 48.

ⁱReference 52.

^jReference 53.

the choice of d_0 from 20 to 44 eV. Therefore, if one were seeking agreement with data on the r factor for Si a variation of d_0 alone would not be a large degree of freedom; the acoustic-phonon deformation-potential parameters would also play a role even at 300 K.

In selecting a value of d_0 I was confronted by a large disparity between various published results. Table IV gives the values of various parameters for high-purity p -type Si found in the literature. The μ_c values quoted are from minority carrier drift measurements on n -type Si. In this case it is preferred to use μ_H values. The most recent values for μ_H are both around 370 cm²/V sec. The measurements of Baron *et al.*⁵² are particularly careful since in their study they considered the effects of surface preparation and used high-purity Si:B samples: $N_A = 5 \times 10^{11}$ cm⁻³ and $N_D = 1.1 \times 10^{11}$ cm⁻³. With μ_H (300 K) = 370 cm²/V sec, from Fig. 9 $d_0 = 29.3$ eV, $\mu_c = 505$ cm²/V sec, and $r(300 \text{ K}) = 0.73$. For comparison, with $d_0 = 26.2$ eV, $\mu_H(300 \text{ K}) = 412$ cm²/V sec of Elstner,⁵³ with $\mu_c(300 \text{ K}) = 554$ cm²/V sec, and $r(300 \text{ K}) = 0.744$. The choice of $d_0 = 29.3$ eV is consistent with the typical $d_0 = 30$ –40 eV values found for most group IV and III-V semiconductors.²⁵ The value of $\mu_c = 505$ cm²/V sec is also consistent with the drift-mobility measurements in Table IV. Results for the r factor will also be shown later to be in good agreement with the data.

Figure 10 provides the total and partial conductivity mobilities for p -type Si and comparison with data. The lower-temperature region is compared with the data of Mitchel and Hemenger.¹ Above 100 K the data of Ludwig and Watters⁴⁶ is used. Table V summarizes the relative importance of the three bands to the overall conductivities. Apparently, the H -hole band dominates the conductivity mobility. The calculated μ_c exhibits a slight tailing effect for $T > 300$ K which is not seen in the data of Ludwig and Watters⁴⁶ but can be seen in μ_H data for sample $B-8$ of Braggins,⁵⁴ $N_A = 1.5 \times 10^{14}$ cm⁻³, $N_D = 5 \times 10^{12}$ cm⁻³. It is also a feature in calculated curves of Nakagawa and Zukotynski,²⁴ Takeda *et al.*,²⁶ and Jacoboni *et al.*⁵⁵ It is not clear whether the effect is a true one or simply connected with inadequacies of the $6 \times 6 \vec{k} \cdot \vec{p}$ Hamiltonian for higher energies.⁴⁴ The relative constancy of the hole population ratios for the H -hole and L -hole band is indicative of the parabolic band behavior at higher energies, Table V. Nevertheless, the agreement be-

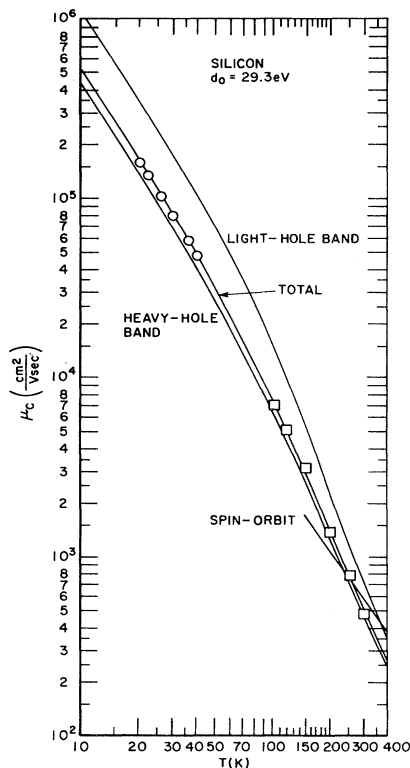


FIG. 10. Total and partial conductivity mobilities and experimental results in the phonon-limited regime for p -type Si with $d_0 = 29.3$ eV as a function of temperature. The circles represent sample 1202- H , Hall bar of Mitchel and Hemenger (Ref. 1), $N_A = 6.57 \times 10^{11}$ cm $^{-3}$, $N_D = 3.96 \times 10^{11}$ cm $^{-3}$ and the squares represent the Ludwig and Watters (Ref. 46) minority carrier drift mobility on n -type samples with resistivities between 19–180 Ω cm.

tween experiment and theory in Fig. 10 is very good even though the data of Ludwig and Watters⁴⁶ has $\mu_c(300$ K) $=485$ and the fit for d_0 uses $\mu_c(300$ K) $=505$ cm 2 /V sec. For comparison with entries in Table V, Nakagawa and Zukotynski²⁴ obtain $\sigma_{11}^H/\sigma_{11}^L=2.56$ at 60 K, 4.55 at 300 K; $\sigma_{123}^L/\sigma_{123}^H=2.37$ at 60 K and 1.40 at 300 K. This is in agreement with the general trend but with much slower temperature dependence than in Table V.

Figure 11 presents results for the total and partial Hall mobilities together with the data of Mitchel and Hemenger¹ on sample 1202- H . From Table V it is seen that the L -hole band governs the behavior of the μ_H more than the H -hole band, but only in the acoustic-phonon-limited regime. In the optical-phonon-limited regime it is the H -hole band which again dominates μ_H . This is in sharp contrast to the situation for Ge, Table III, where it is the H -hole band for μ_c and L -hole band for μ_H which are most significant over the entire temperature range. This different behavior will be seen to account for different shapes of the resultant r factors. Again the data do not exhibit the slight bowing in the calculated curve. It should be said that the particular sample used for comparison is so pure that it becomes intrinsic at about 350 K. Therefore, the apparent Hall mobilities may be somewhat depressed in value owing to cancellation of the Hall voltage by intrinsic electrons.⁵⁶ If this effect were to be corrected, the high-temperature end of the data would be raised somewhat to produce the predicted bowing of the mobility. The sample VS14 ($N_A = 1 \times 10^{13}$ cm $^{-3}$, $N_D = 6.5 \times 10^{10}$ cm $^{-3}$) of Elstner⁵³ does exhibit the bowing for $T > 250$ K perhaps because it is doped higher than the sample 1202- H of Mitchel and Hemenger and does not convert in type close to the room temperature. The agreement between experiment and theory is seen to be very good. It is especially important that with one fitting parameter, d_0 at 300 K, the break in the μ_H curve at the onset of strong optical-phonon scattering is reproduced correctly, as is the curve beyond the break. Below the break the agreement with the data has already been demonstrated in Refs. 2 and 3.

In Fig. 12 the calculated temperature exponents of both mobilities are shown. At the very lowest of temperature there is good agreement with the data of Mitchel and Hemenger.¹ The average exponent in the (100–300)-K range was calculated to be $\bar{\alpha}_c = 2.4$ and $\bar{\alpha}_H = 2.9$. This is to be compared with the measured values in Table IV which are $\alpha_c \sim 2.2$ – 2.3 , 2.7 ± 0.1 , and $\alpha_H \sim 2.9$ – 3.0 . The theory indicates that exponents have an appreciable temperature dependence. At higher temperatures this dependence is the consequence of the bowing effect discussed above. Since experiments typically extract only one exponent, the comparison with the average values $\bar{\alpha}_{c,H}$ appears to be more relevant.

Figure 13 gives the calculated r factor for three choices

TABLE V. Ratios of band contributions to the conductivity tensors in Si, $d_0 = 29.3$ eV.

T (K)	$\sigma_{11}^H/\sigma_{11}^L/\sigma_{11}^S$	$\sigma_{123}^L/\sigma_{123}^H/\sigma_{123}^S$	$p_H/p_L/p_S$
10	2.57:1	1.74:1	6.40:1
50	2.93:1	2.07:1	7.52:1
100	3.74:1:0.0011	2.04:1:0.0003	8.84:1:0.0063
150	4.64:1:0.0106	1.71:1:0.0034	9.37:1:0.0294
200	5.40:1:0.0285	1.25:1:0.0115	9.49:1:0.0566
250	5.93:1:0.0547	0.96:1:0.0224	9.46:1:0.0864
300	6.28:1:0.0861	0.77:1:0.0364	9.39:1:0.104
350	6.50:1:0.118	0.67:1:0.0506	9.31:1:0.121
400	6.64:1:0.146	0.59:1:0.0654	9.24:1:0.135

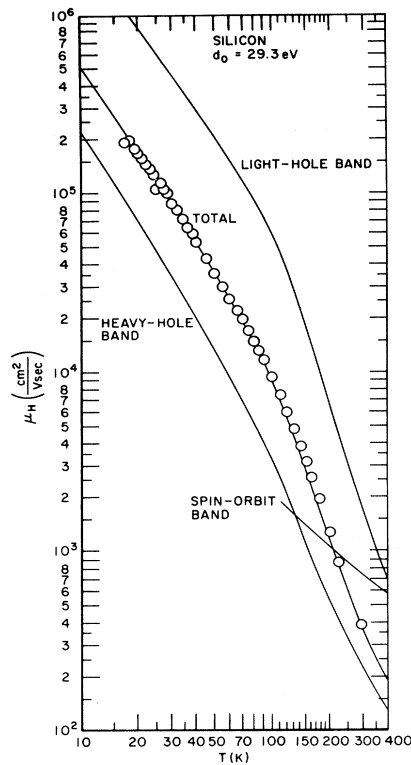


FIG. 11. Total and partial Hall mobilities with experimental data in the phonon-limited regime for *p*-type Si with $d_0=29.3$ eV as a function of temperature. The circles represent the data of Mitchel and Hemenger (Ref. 1), sample 1202-*H*.

of d_0 . At lower temperatures the three curves are the same, but with the onset of optical-phonon scattering important differences arise. The r factor at low temperatures is within 4% of the values for samples 1202-*H* and 1300-*V* of Mitchel and Hemenger.¹ There is a conspicuous absence of data in the intermediate-temperature range. The

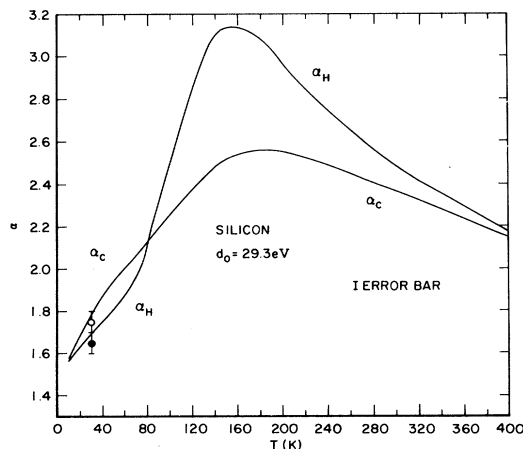


FIG. 12. Temperature exponents (dimensionless) for the conductivity and Hall mobilities, α_c and α_H , respectively, for *p*-type Si with $d_0=29.3$ eV. The closed circle represents $\alpha_c=1.75\pm 0.05$ and the open circle represents $\alpha_H=1.65\pm 0.05$ of Mitchel and Hemenger (Ref. 1).

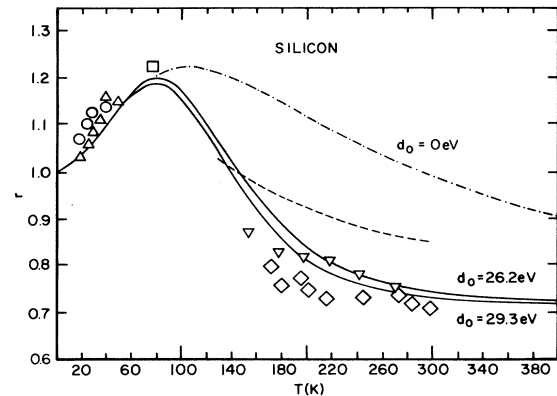


FIG. 13. Calculated and experimental r factor for *p*-type Si. The circles represent Mitchel and Hemenger (Ref. 1), sample 1202-*H*, $N_A=6.57\times 10^{11}$ cm⁻³, $N_D=3.96\times 10^{11}$ cm⁻³. The triangles represent Mitchel and Hemenger (Ref. 1), sample 1300-*V*, van der Pauw configuration, $N_A=9.14\times 10^{11}$ cm⁻³, $N_D=3.33\times 10^{11}$ cm⁻³. The square represents Reid and Willardson (Ref. 57), sample 8A, 2700 Ω cm $\sim N_A-N_D=4\times 10^{12}$ cm⁻³. The inverted triangles represent Long (Ref. 58), 35 Ω cm $\sim N_A-N_D=3.5\times 10^{14}$ cm⁻³. The diamonds represent Morin and Maita (Ref. 49), sample 127, $N_A=7.0\times 10^{14}$ cm⁻³, $N_D=2.2\times 10^{14}$ cm⁻³. The dashed curve represents Messier and Flores (Ref. 51), 6200 Ω cm $\sim N_A-N_D=2\times 10^{12}$ cm⁻³.

lone data point of Reid and Willardson⁵⁷ makes it plausible that the r factor should still rise until at least 77 K. Given the 0.7–0.8 measured r values^{49,58} for $T > 150$ K, the r factor should peak and fall off, but the peak value and the rate of fall cannot be compared with experiment.

At higher temperatures the data of Morin and Maita,⁴⁹ Messier and Flores,⁵¹ and of Long⁵⁸ are given. The data of Messier and Flores⁵¹ employ $\mu_H(300\text{ K})=398$ cm²/V sec which is larger than $\mu_H=370$ cm²/V sec used here. Also they use $\mu_c(300\text{ K})=471$ cm²/V sec of Ludwig and Watters⁴⁶ (from the $\mu_c=2.3\times 10^9 T^{-2.7}$ expression⁴⁶) compared to $\mu_c(300\text{ K})=505$ cm²/V sec used here. As a consequence Messier and Flores⁵¹ obtain $r(300\text{ K})=0.84$, about 14% higher than $r(300\text{ K})=0.73$ in Fig. 11. The data of Morin and Maita⁴⁹ was taken using $\mu_c(300\text{ K})=500$ cm²/V sec of Prince⁴⁵ which is consistent with $\mu_c(300\text{ K})=505$ cm²/V sec calculated with $d_0=29.3$ eV. With these provisos it can be concluded that the calculated high-temperature r factor is in good agreement with the data. A comparison with the data of Messier and Flores⁵¹ is complicated by their use of the $\alpha_c=2.7$ exponent from Ludwig and Watters,⁴⁶ a lower μ_c and higher μ_H than used here. It is possible to calculate the r factor from the Hall coefficient of Messier and Flores,⁵¹ $R_H=r/qp$, by assuming that for $T > 150$ K p is constant (as was done by Long and Brown and Bray), and normalizing this r to 0.73 at 300 K. By this procedure agreement with the theory is very much improved for the shape of the r factor. The assumption that p is constant should break down below the exhaustion ration, $T < 150$ K, or so.

From Table V the falloff of the r factor at higher temperatures is due to the increase in the importance of the *H*-hole band to μ_H while its importance to μ_c is relatively

constant. Therefore, $r = \mu_H / \mu_c$ decreases since H holes are less mobile than the L holes. This effect is much stronger in this calculation than predicted by Nakagawa and Zukotynski²⁴ and accounts for the relatively sharper peak in Fig. 13 for the r factor. Nakagawa and Zukotynski²⁴ indicated that the temperature dependence of the r factor can be understood in terms of band warpage or anisotropy. A band with large anisotropy, such as the heavy-hole band of Si, tends to decrease the r factor with temperature while the more isotropic L -hole band tends to increase it. These two effects compete since the degree of warpage in the H -hole band of Si increases with hole energy⁶ so that at higher temperatures the total r factor decreases.

This type of behavior is consistent with observations made by Allgaier⁵⁹ who examined the effect of anisotropy of constant-energy surfaces on the r factor. His general conclusion was that the band-shape anisotropy decreases the r factor while the anisotropy in the scattering rates increases it. In the optical-phonon region the rates are effectively isotropic for p -type Si so that the band anisotropies are the determining factors. The H -hole band in Si is more warped at higher energies which depresses the r factor due to both the acoustic and optical processes.

The anisotropy of the valence bands in Ge is small in comparison to Si bands. Here it is the band nonparabolicity which governs the shape of the mobility and r -factor curves. Owing to the large spin-orbit splitting energy, the nonparabolicity of the L -hole band persists to higher energies in Ge than in Si, which makes the r factor rise in Fig. 6. All these effects are only qualitative in nature and must be tested on each real system.

In indirect support of the r factor in Fig. 11, Hall-data analysis for sample 1202- H of Mitchel and Hemenger⁵⁶ was performed with the calculated r factor. The low-temperature r factor was already shown to correct for the "spike" anomaly in the p vs $1/T$ curve.¹ The addition of the calculated $50 < T < 400$ K r factor in the analysis extended the boron exhaustion plateau up to about 300 K, near the onset of intrinsic conduction. The plateau was flat which indicates that the r factor has considerable numerical accuracy. (It also indicates the absence of any significant amounts of impurities deeper than boron in the sample.)

V. SUMMARY AND CONCLUSIONS

The conductivity and Hall mobilities for p -type silicon and germanium have been calculated in both the acoustic and optical-phonon-limited regimes. The model involved accurate band dispersions for all three top valence bands, the deformation-potential theory for calculating phonon-hole transition rates, and the solution of the full Boltzmann equation.

The one fitting parameter d_0 used to adjust the strength of hole-optical-phonon interaction was within the range of independent estimates of its value. This fact lends support for the physical basis of the deformation-potential theory.

Results of the calculation are most strenuously tested when the calculated r factors are compared with experi-

ments. The theoretical r factors were shown to be consistent with experimental data. The agreement for Si is very good at low temperatures; at higher temperatures substantial agreement is found with two sets of data. The present model has thus considerably reduced the existing disparity between experiment and theory. By comparison, the r factors for p -type Si by Takeda *et al.*²⁶ and Hackmann *et al.*¹⁸ do not conform even qualitatively to the measured r factor. Results of Nakagawa and Zukotynski²⁴ do much better in this regard, except at lower temperatures. The present model predicts a sharper peak in the r factor than that of Nakagawa and Zukotynski, in better agreement with experiments. The origin of different temperature behavior for the r factor of p -type Si and p -type Ge has been explained in terms of competing effects of the L -hole and H -hole bands. This fact has also been explained by Nakagawa and Zukotynski in terms of band warpage and band nonparabolicity. Use of the calculated r factor has resulted in improved Hall-data fits for high-purity p -type Si.

Owing to as yet an unresolved situation regarding values of acoustic deformation-potential parameters, agreement with data for p -type Ge is less satisfactory. The conductivity mobility is well predicted. The Hall-mobility and the r -factor results are in substantial agreement with the data, on the order of 20% at higher temperatures. This is an improvement on an earlier calculation where errors on the order of 50% arose.²⁴ The present set of deformation-potential parameters works well but clearly is not the optimal set.

Overall, it appears that only more rigorous models of phonon-limited transport can resolve fine details of the mobility curves and particularly of the r factor. Although many band details influence results through band dispersions alone, appreciable band effects are also contained in the transition probabilities. Apparently, the deformation-potential theory takes these well into account. It is also the experience of this calculation that the steady-state distribution functions have important high angular momentum components beyond $l = 1$. This fact restricts the limits of validity for the relaxation-time approach to mobility calculations in p -type Si and p -type Ge.

ACKNOWLEDGMENTS

This work was performed under U. S. Air Force Contract No. F33615-81-C-5095 at the Materials Laboratory, Wright-Patterson Air Force Base, Ohio. Helpful discussions with Dr. P. M. Hemenger, Dr. W. C. Mitchel, Mr. K. Beasley, and Mr. J. A. Detrio are gratefully acknowledged. The author is indebted to Dr. F. L. Madarasz for his involvement in the initial stages of the work leading up to the present paper.

APPENDIX A

The factor of $\frac{1}{2}$ in front of Eq. (2.35) is due to the structure of the Boltzmann equation

$$\mathcal{F}f_n(\vec{k}) = \frac{\Omega}{(2\pi)^3} \sum_m \int d\vec{k}' [P_{mn}(\vec{k}', \vec{k})f_m(\vec{k}') - P_{nm}(\vec{k}, \vec{k}')f_n(\vec{k})], \quad (\text{A1})$$

where \mathcal{F} stands for the field operators, P for the transition rates, and f are the distribution functions. The band indices n, m single out individual members of the degenerate band manifolds. Since the scattering mechanisms considered here do not affect the carriers' spin $f_n(\vec{k}) = f_m(\vec{k})$ as long as n and m are within the same degenerate manifold, $N(n) = N(m)$. To cut the task of solving Eq. (A2) in half one may sum Eq. (A2) over the members of the same manifold $n(N)$

$$\mathcal{F} \sum_{n(N)} f_n(\vec{k}) = \frac{\Omega}{(2\pi)^3} \sum_{m(N)} \sum_{n(N)} \int d\vec{k}' [P_{mn}(\vec{k}', \vec{k}) f_m(\vec{k}') - P_{nm}(\vec{k}, \vec{k}') f_n(\vec{k})]. \quad (\text{A2})$$

For a fixed manifold index N , and $n(N) = p(N)$, we have

$$f_{n(N)} = f_{p(N)} \equiv \frac{f_N}{2}, \quad (\text{A3})$$

so that Eq. (A2) becomes

$$\mathcal{F} f_N(\vec{k}) = \frac{\Omega}{(2\pi)^3} \sum_{m(N)} \sum_{n(N)} \int d\vec{k}' [P_{mn}(\vec{k}', \vec{k}) f_m(\vec{k}') - \frac{1}{2} P_{nm}(\vec{k}, \vec{k}') f_N(\vec{k})]. \quad (\text{A4})$$

The sum over m proceeds over all available indices so that

$$\sum_m = \sum_M \sum_{m(M)} \quad (\text{A5})$$

and

$$f_m = f_{m(M)} = \frac{1}{2} f_M. \quad (\text{A6})$$

The structure of the Boltzmann equation can now be written as

$$\mathcal{F} f_N(\vec{k}) = \frac{\Omega}{(2\pi)^3} \sum_M \int d\vec{k}' [P_{MN}(\vec{k}', \vec{k}) f_M(\vec{k}') - P_{NM}(\vec{k}, \vec{k}') f_N(\vec{k})], \quad (\text{A7})$$

where

$$P_{NM}(\vec{k}, \vec{k}') = \frac{1}{2} \sum_{n(N)} \sum_{m(M)} P_{nm}(\vec{k}, \vec{k}'), \quad (\text{A8})$$

and Eq. (A8) explains the factor of $\frac{1}{2}$ in Eq. (2.35). The distribution functions $f_N(\vec{k})$ take into account the band occupancy including spin, so that the thermal equilibrium function is

$$f_N^0(\vec{k}) = 2 \left[\exp \left[\frac{E_N(\vec{k}) - \mu}{k_B T} \right] + 1 \right]^{-1}, \quad (\text{A9})$$

where μ is the chemical potential. Therefore, the exclusion principle in the scattering term of the Boltzmann equation, Eq. (2.44), will have the form

$$\left[1 - \frac{1}{2} f_N(\vec{k}) \right], \quad (\text{A10})$$

so that scattering into band N at \vec{k} is forbidden if the level is doubly occupied.

APPENDIX B

The expression for the hole-optical-phonon scattering rate of Bir and Pikus²¹ in the case of two parabolic bands, heavy and light, can be expanded analytically in the double-cubic-harmonic series. Although Lawaetz⁹ provides the result, he does not provide the derivation, which is given below.

We need a double-cubic-harmonic decomposition of the following analytic expression:

$$U^0(\lambda, \hat{k}; \lambda', \hat{k}') = D^2 d_0^2 \frac{\hat{k}_x \hat{k}_y \hat{k}'_x \hat{k}'_y + (\text{c.p.})}{E_{\hat{k}\lambda} E_{\hat{k}'\lambda'}} + \frac{3}{2} d_0^2 - 3d_0^2 \frac{D^2(\hat{k} \cdot \hat{k}')^2 - B^2 + (3B^2 - D^2)[\hat{k}_x^2 \hat{k}'_x{}^2 + (\text{c.p.})]}{4E_{\hat{k}\lambda} E_{\hat{k}'\lambda'}}, \quad (\text{B1})$$

which is proportional to the scattering rate.⁹ In Eq. (B1) B , C , and D are band-shape parameters; \hat{k}_x , \hat{k}_y , and \hat{k}_z are components of the unit vector \hat{k} , c.p. stands for the cyclic permutation of coordinates, and

$$E_{\hat{k}\lambda} = (-1)^\lambda \{ B^2 + C^2 [\hat{k}_x^2 \hat{k}_y^2 + (\text{c.p.})] \}^{1/2}, \quad (\text{B2})$$

where $\lambda = 1, 2$ represents the heavy- and light-hole bands, respectively. For the mobility calculations we only need the cubic-harmonic expansion of U^0 in terms of the Γ_1 cubic harmonic

$$\frac{U^0(\lambda, \hat{k}; \lambda', \hat{k}')}{d_0^2} = \sum_{L, L'} B_{\lambda L, \lambda' L'}^\alpha K_L^\alpha(\hat{k}) K_{L'}^\alpha(\hat{k}') + \dots, \quad (\text{B3})$$

where the ellipsis stands for other even representations and d_0^2 has been factored out to be consistent with Eq. (2.50).

Clearly,

$$d_0^2 B_{\lambda L, \lambda' L'}^\alpha = \int d\hat{k} \int d\hat{k}' U^0(\lambda, \hat{k}; \lambda', \hat{k}') K_L^\alpha(\hat{k}) K_{L'}^\alpha(\hat{k}'), \quad (\text{B4})$$

with two solid-angle integrations of Eq. (B1). First, note that $E_{\hat{k}\lambda}$ in Eq. (B3) transforms according to the invariant representation Γ_1 . The numerator of the first term in Eq. (B1) transforms as xy , yz , and xz according to the ϵ or Γ_{25}^{\prime} representation in both \hat{k} and \hat{k}' . Therefore, the solid-angle integrals in Eq. (B4) with the Γ_1 cubic harmonics yield zero for the first term of Eq. (B1). The second term of Eq. (B1) yields the following contribution to $B_{\lambda L, \lambda' L'}^\alpha$:

$$B_{\lambda L, \lambda' L'}^\alpha = 6\pi \delta_{L0} \delta_{L'0}. \quad (\text{B5})$$

The third term in Eq. (B1) contributes exactly zero to

$B_{\lambda L, \lambda' L'}^{\alpha}$. This can be seen simply as follows. The $(\hat{k} \cdot \hat{k}')$ term, when expanded, becomes

$$(\hat{k} \cdot \hat{k}')^2 = (\hat{k}_x^2 \hat{k}'_x{}^2 + \text{c.p.}) + 2(\hat{k}_x \hat{k}'_y \hat{k}_y \hat{k}'_x + \text{c.p.}). \quad (\text{B6})$$

The cross terms in Eq. (B6) drop out from the integration since they transform according to the Γ_{25} representation. The first term in Eq. (B6) cancels exactly the $(-D^2)$ term in Eq. (B1). What remains is to integrate

$$3 \frac{B^2 - 3B^2(\hat{k}_x^2 \hat{k}'_x{}^2 + \hat{k}_y^2 \hat{k}'_y{}^2 + \hat{k}_z^2 \hat{k}'_z{}^2)}{4E_{\hat{k}\lambda} E_{\hat{k}'\lambda'}} K_L^{\alpha}(\hat{k}) K_L^{\alpha}(\hat{k}'), \quad (\text{B7})$$

over both solid angles. The first term of Eq. (B7) is identical in each of the 48 irreducible wedges W of the Brillouin zone and is equal to

$$3B^2(48 \times 48) \int_W d\hat{k} \int_W d\hat{k}' \frac{K_L^{\alpha}(\hat{k}) K_L^{\alpha}(\hat{k}')}{4E_{\hat{k}\lambda} E_{\hat{k}'\lambda'}}, \quad (\text{B8})$$

The second term of Eq. (B7) can be similarly written out in terms of its contribution from all the irreducible wedges; the result is exactly negative to Eq. (B8). Therefore, Eq. (B5) gives the only cubic-harmonic expansion coefficient for the α representation in the analytic case.⁹

APPENDIX C

The approximation for the Bose-Einstein phonon distribution function

$$n_0 = \left[\exp \left(\frac{\hbar\omega}{k_B T} \right) - 1 \right]^{-1} \simeq \frac{k_B T}{\hbar\omega} \equiv x \quad (\text{C1})$$

is strictly valid only for $k_B T \gg \hbar\omega$. Question may be raised whether this approximation is valid for the treat-

ment of the acoustic-phonon—hole scattering in this paper and in Refs. 2–4 and 9.

From conservation of energy and momentum one can show that the typical phonon energy is given by⁹

$$\hbar\omega = \hbar c q = 2m^* c^2, \quad (\text{C2})$$

where c is the average long-wavelength phonon speed and m^* is the hole's effective mass. For silicon, in the worst case $m^* \simeq 0.5m_0$ for the heavy-hole band and $c \simeq 7 \times 10^5$ cm/sec. Therefore, $\hbar\omega \simeq 2.8 \times 10^{-4}$ eV, equivalent to about 3 K, which validates the idea of elastic hole scattering. But, at 20 K, where typically first experimental data points are used for comparison,

$$x = 6.2, \quad (\text{C3})$$

which gives an 8% error in the equipartition approximation, Eq. (C1). At 10 K the error is 18%.

The approximation employed here goes beyond the equipartition expansion of n_0 ,

$$n_0 = x \left[1 - \frac{1}{2x} + \frac{1}{12x^2} + \dots \right] \simeq x. \quad (\text{C4})$$

The transition rates for the emission and absorption of acoustic phonons are taken to be the same apart from the phonon occupancy factors, that is,

$$\text{Rate} \sim (n_0 + 1) + n_0, \quad (\text{C5})$$

for emission plus absorption, respectively. The approximation that is being used is

$$(n_0 + 1) + n_0 = 2x \left[1 + \frac{1}{12x^2} + \dots \right] \simeq 2x, \quad (\text{C6})$$

which at 10 K is good to 0.9% and at 20 K is good to 0.2%. This then is decidedly better than the equipartition approximation alone.

- ¹W. C. Mitchel and P. M. Hemenger, *J. Appl. Phys.* **53**, 6880 (1982).
²F. Szmulowicz and F. L. Madarasz, *Phys. Rev. B* **27**, 2605 (1983).
³F. Szmulowicz and F. L. Madarasz, *Phys. Rev. B* **27**, 6279 (1983).
⁴M. Tiersten, *IBM J. Res. Dev.* **5**, 122 (1961).
⁵M. Tiersten, *J. Phys. Chem. Solids* **25**, 1151 (1964).
⁶E. O. Kane, *J. Phys. Chem. Solids* **1**, 82 (1956).
⁷F. L. Madarasz and F. Szmulowicz, *Phys. Rev. B* **24**, 4611 (1981).
⁸F. Szmulowicz and F. L. Madarasz, *Phys. Rev. B* **26**, 2101 (1982).
⁹P. Lawawtz, *Phys. Rev.* **174**, 867 (1968).
¹⁰Albert C. Beer, in *Galvanomagnetic Effects in Semiconductors*, Suppl. 4 of *Solid State Physics*, edited by F. Seitz and D. Turnbull (Academic, New York, 1963), p. 287. There are added complications in the use of the relaxation-time concept if collisions are nonelastic and nonrandomizing or if the energy surfaces are not quadratic.
¹¹H. Ehrenreich and A. W. Overhauser, *Phys. Rev.* **104**, 331 (1956); **104**, 649 (1956).

- ¹²J. Bardeen and W. Shockley, *Phys. Rev.* **80**, 72 (1950).
¹³E. M. Conwell, *Sylvania Technol.* **12**, 30 (1959); in *High Field Transport in Semiconductors*, Suppl. 9, of *Solid State Physics*, edited by F. Seitz, D. Turnbull, and H. Ehrenreich (Academic, New York, 1967); *J. Phys. Chem. Solids* **8**, 234 (1959).
¹⁴J. D. Wiley and M. DiDomenico Jr., *Phys. Rev. B* **2**, 427 (1970).
¹⁵D. M. Brown and R. Bray, *Phys. Rev.* **127**, 1593 (1962).
¹⁶J. F. Lin, S. S. Li, L. C. Linares, and K. W. Teng, *Solid-State Electron.* **24**, 827 (1981).
¹⁷G. L. Bir, E. Normantas, and G. E. Pikus, *Fiz. Tverd. Tela (Leningrad)* **4**, 1180 (1962) [*Sov. Phys.—Solid State* **4**, 867 (1962)].
¹⁸A. Hackmann, D. Neubert, U. Scherz, and R. Schlieff, *Phys. Rev. B* **24**, 4666 (1981).
¹⁹J. D. Wiley, *Phys. Rev. B* **4**, 2485 (1971); in *Transport Phenomena*, Vol. 10 of *Semiconductors and Semimetals*, edited by R. K. Willardson and A. C. Beer (Academic, New York, 1975), also good for review of transport theory up to 1975; *Solid State Commun.* **8**, 1865 (1970).
²⁰C. Herring and E. Vogt, *Phys. Rev.* **101**, 944 (1956). This reference also contains a discussion of applicability of the

- relaxation-time approximation.
- ²¹G. L. Bir and G. E. Pikus, *Fiz. Tverd. Tela (Leningrad)* **2**, 2287 (1960) [*Sov. Phys.—Solid State* **2**, 2039 (1961)].
- ²²G. E. Pikus and G. L. Bir, *Fiz. Tverd. Tela (Leningrad)* **1**, 1642 (1959); **1**, 1828 (1959) [*Sov. Phys.—Solid State* **1**, 1502 (1960); **1**, 1675 (1960)].
- ²³M. Costato, G. Gagliani, C. Jacoboni, and L. Reggiani, *J. Phys. Chem. Solids* **35**, 1605 (1974).
- ²⁴H. Nakagawa and S. Zukotynski, *Can. J. Phys.* **55**, 1485 (1977); **56**, 364 (1977).
- ²⁵F. Meseguer, J. C. Merle, and M. Cardona, *Solid State Commun.* **43**, 511 (1982). The four basic deformation potentials a , b , d , and d_0 may also be related to the phenomenological deformation potentials as shown by Lawaetz (unpublished); see J. D. Wiley, *Solid State Commun.* **8**, 1865 (1970). This procedure though is only valid for parabolic bands.
- ²⁶K. Takeda, K. Sakui, and M. Sakata, *J. Phys. C* **15**, 767 (1982).
- ²⁷G. L. Bir and G. E. Pikus, *Symmetry and Strain-Induced Effects in Semiconductors* (Wiley, New York, 1974).
- ²⁸D. L. Rode, in *Transport Phenomena*, Vol. 10 of *Semiconductors and Semimetals*, edited by R. K. Willardson and A. C. Beer (Academic, New York, 1975).
- ²⁹P. Lawaetz, *Phys. Rev.* **166**, 763 (1968).
- ³⁰J. F. Cornwell, *Group Theory and Electronic Energy Bands in Solids* (Wiley, New York, 1969).
- ³¹S. M. Sze, *Physics of Semiconductor Devices* (Wiley, New York, 1969), pp. 57–58.
- ³²L. M. Roth, B. Lax, and S. Zwerdling, *Phys. Rev.* **114**, 90 (1959).
- ³³F. C. Von der Lage and H. Bethe, *Phys. Rev.* **71**, 612 (1947).
- ³⁴S. L. Altmann and A. P. Cracknell, *Rev. Mod. Phys.* **37**, 19 (1965).
- ³⁵P. J. Davis and I. Polonski, in *Handbook of Mathematical Functions with Formulas, Graphs, and Mathematical Tables*, edited by M. Abramowitz and I. A. Stegun (U. S. GPO, Washington, D.C., 1972), p. 678.
- ³⁶A. H. Stroud and D. Secrest, *Gaussian Quadrature Formulas* (Prentice-Hall, Englewood Cliffs, 1966), p. 253.
- ³⁷M. B. Prince, *Phys. Rev.* **92**, 681 (1953).
- ³⁸G. Ottaviani, C. Canali, F. Nava, and J. W. Mayer, *J. Appl. Phys.* **44**, 2917 (1973).
- ³⁹P. Lawaetz, *Phys. Rev.* **183**, 730 (1969).
- ⁴⁰L. Reggiani, C. Canali, F. Nava, and G. Ottaviani, *Phys. Rev. B* **16**, 2781 (1977).
- ⁴¹C. Goldberg, E. N. Adams, and R. E. Davis, *Phys. Rev.* **105**, 865 (1957).
- ⁴²A. C. Beer and R. K. Willardson, *Phys. Rev.* **110**, 1286 (1958).
- ⁴³F. J. Morin, *Phys. Rev.* **93**, 62 (1954).
- ⁴⁴R. G. Humphreys, *J. Phys. C* **14**, 2935 (1981).
- ⁴⁵M. B. Prince, *Phys. Rev.* **93**, 1204 (1954).
- ⁴⁶G. W. Ludwig and R. L. Watters, *Phys. Rev.* **101**, 1699 (1956).
- ⁴⁷D. Cronmeyer, *Phys. Rev.* **105**, 522 (1957).
- ⁴⁸G. Ottaviani, L. Reggiani, C. Canali, F. Nava, and A. Alberigi-Quaranta, *Phys. Rev. B* **12**, 3318 (1975).
- ⁴⁹F. J. Morin and J. P. Maita, *Phys. Rev.* **96**, 28 (1954).
- ⁵⁰P. P. Debye and T. Kohane, *Phys. Rev.* **94**, 724 (1954).
- ⁵¹J. Messier and J. M. Flores, *J. Phys. Chem. Solids* **24**, 1539 (1963).
- ⁵²R. Baron, M. H. Young, J. K. Neeland, and O. Y. Marsh, in *Semiconductor Silicon 1977*, edited by H. R. Huff and E. Sirtl (Electrochemical Society, Princeton, 1977), pp. 367–376.
- ⁵³L. Elstner, *Phys. Status Solidi* **17**, 139 (1966).
- ⁵⁴T. T. Braggins, Ph.D. thesis, Syracuse University (University Microfilms, Ann Arbor, Michigan, 1975), pp. 73 and 76 (unpublished).
- ⁵⁵C. Jacoboni, C. Canali, G. Ottaviani, and A. Alberigi-Quaranta, *Solid-State Electron.* **20**, 77 (1977).
- ⁵⁶W. C. Mitchel, P. M. Hemenger, and K. Beasley (private communication).
- ⁵⁷F. J. Reid and R. K. Willardson (unpublished); in *Galvanomagnetic Effects in Semiconductors*, Suppl. 4 of *Solid State Physics*, Ref. 10, p. 209.
- ⁵⁸D. Long, *Phys. Rev.* **107**, 672 (1957).
- ⁵⁹R. S. Allgaier, *Phys. Rev. B* **2**, 3869 (1970).